Zinc controls histone acetyltransferase KAT7 activity to maintain cellular zinc homeostasis

Takao Fujisawa[1,*,†], Satoshi Takenaka[1,*], Lila Maekawa[1], Toshiyuki Kowada[2], Toshitaka Matsui[2], Shin Mizukami[2], Isao Naguro[1], and Hidenori Ichijo[1,†]

[1]Laboratory of Cell Signaling, Graduate School of Pharmaceutical Sciences, The University of Tokyo, Tokyo 113-0033, Japan
[2]Institute of Multidisciplinary Research for Advanced Materials, Tohoku University, 2-1-1 Katahira, Aoba-ku, Sendai, Miyagi 980-8577, Japan.

*These authors equally contributed to this work.
[†]Correspondence: fujisawa@mol.f.u-tokyo.ac.jp, ichijo@mol.f.u-tokyo.ac.jp

Abstract

Zinc is an indispensable micronutrient for optimal physiological function; therefore, zinc deficiency has been implicated in the pathogenesis of various human diseases. To address these deleterious conditions, our bodies have regulatory mechanisms that respond to zinc deficiency stress at the cellular level. However, the related molecular mechanisms, especially at the gene expression level, remain poorly understood. Here, we show that during zinc deficiency, the histone acetyltransferase KAT7 loses its enzymatic activity, leading to the attenuated acetylation of histone H3 at Lys14 (H3K14ac). Physiologically, this decrease in H3K14ac leads to the transcriptional upregulation of *ZIP10*, a plasma membrane-localized zinc transporter, thereby importing zinc from extracellular sources to maintain cellular zinc homeostasis. Our data demonstrate that cells respond to zinc deficiency stress by converting it into an epigenetic signal to drive cellular responses.

Main

Zinc is an essential micronutrient that plays a pivotal role in maintaining the structural integrity and enzymatic activities of numerous proteins. Computational analysis reports that as much as 10% of the human genome encodes a zinc-binding proteins[1], suggesting the importance of maintaining zinc homeostasis in our body. Nevertheless, we suffer from zinc deficiency, which can arise from various factors such as inadequate zinc intake, impaired zinc absorption, and ageing[2]. The clinical manifestations of zinc deficiency in humans were first reported in the 1960s[3,4], and since then, numerous studies have shown that zinc deficiency is strongly associated with the development of various diseases including skin diseases and cancers, as well as immune dysfunction and growth retardation[5].

To overcome zinc-deficient conditions, cells need to import zinc from extracellular sources. The Zrt-/Irt-like protein (ZIP) family is a group of zinc ion transporters[6]. Among the 14 human ZIP family proteins, 10 ZIPs (ZIP1-6, 8, 10, 12, and 14) are thought to be localized on the plasma membrane and be involved in the import of extracellular zinc. Upon zinc deficiency, the abundance of ZIPs on the plasma membrane increases to facilitate zinc uptake as a stress response to maintain cellular zinc homeostasis. One related mechanism involves the upregulation of gene expression through transcriptional control. For example, our previous research has demonstrated

that zinc deficiency activates the transcription factor ATF6 via the endoplasmic reticulum (ER) stress response, thereby promoting the transcription of *ZIP14*[7]. In addition, it has been reported that *ZIP10* exhibits increased expression during zinc deficiency through transcriptional control mediated by the transcription factor MTF1[8]. However, the detailed molecular mechanisms remain largely unclear.

Histone posttranslational modifications (PTMs) are one of the key regulators that govern transcriptional control[9]. Each histone PTM is balanced via the regulation of a myriad of enzymes referred to as "writers" and "erasers"; writers catalyse the formation of specific types of PTMs, and erasers remove the PTMs. Interestingly, multiple writers and erasers possess zinc-binding domains[10], suggesting the critical role of zinc in regulating histone PTMs. Nevertheless, little is known about the dynamics of these writers and erasers during zinc deficiency.

In this study, we report a drastic decrease in histone H3K14ac during zinc deficiency. Mechanistically, this is driven by the loss of activity of a zinc-dependent writer KAT7, which catalyses H3K14ac formation. The decrease in H3K14ac on enhancer regions leads to the upregulation of *ZIP10*, thereby facilitating the import of extracellular zinc. Thus, zinc-dependent regulation of H3K14ac is crucial for maintaining cellular zinc homeostasis.

Results

Global decrease in histone H3K14ac during zinc deficiency

We previously reported that the activation of the transcription factor ATF6 elicits the upregulation of *ZIP14* in HepG2 cells during zinc deficiency[7]. To investigate the impact of ATF6 on global expression changes in genes other than *ZIP14*, we examined the presence of ATF6-binding motifs on the promoters of genes whose expression was upregulated under zinc-deficient conditions. The Gene Expression Omnibus (GEO) repository contains four datasets reporting gene expression profiles in various types of cells during zinc deficiency, including a dataset from our laboratory[7,11–13]. We found that, across all the datasets, fewer than 2% of the genes exhibited the ATF6-binding motif[14] (ER stress-responsive elements, ERSE) within their promoter regions (Extended Data Fig. 1a). This result indicates that there exist mechanisms other than the ATF6-axis which contribute to the alterations in gene expression provoked by zinc deficiency.

In this study, we focused on the role of histone PTMs, which are critical factors responsible for gene expression changes whose association with zinc deficiency remains unexplored. First, we systematically analysed whether zinc deficiency stress affects the major histone PTMs implicated in gene expression in HEK293A cells (promoter marks: H3K4me3, H4K5ac, and H4K12ac, enhancer marks: H3K4me, H3K14ac, and H3K27ac, gene body marks: H3K36me3 and H3K79me3, and heterochromatin marks: H3K9me3 and H3K27me3). We found that treatment with N,N,N',N'-tetrakis(2-pyridylmethyl)ethylenediamine (TPEN), a cell-permeable zinc chelator, selectively attenuated the signal for H3K14ac, but no other marks (Fig. 1a). This reduction in H3K14ac was observed across diverse cellular contexts (Extended Data Fig. 1b,c). This was also evident when cells were cultured in a zinc-deficient medium (Fig. 1b), where the reduction was no longer caused by the addition of zinc and remained unaltered by the addition of other metals (Fig. 1c,d). Furthermore, the H3K14ac signal was restored in a time-dependent manner by the re-supplying zinc after it had been diminished under conditions of zinc deficiency (Fig. 1e). Collectively, these results indicate that zinc exerts regulatory control over H3K14ac.

HDACs deacetylate H3K14ac during zinc deficiency

We next investigated the molecular mechanisms behind the reduction in H3K14ac during zinc deficiency. In general, histone acetylation status is balanced by histone deacetylases (HDACs) and histone acetyltransferases (HATs). We reasoned that the activation of HDACs or the inactivation of HATs results in the decrease in H3K14ac during zinc deficiency.

First, we investigated the involvement of HDACs. HDACs are classified into two distinct categories: the classic HDAC family (HDAC1-11) and the sirtuin family of NAD-dependent HDACs (SIRT1-7). To identify which HDACs are responsible for the deacetylation of H3K14ac during zinc deficiency, we treated the cells with specific inhibitors of each HDAC family. Treatment with nicotinamide (NAM), a pan-inhibitor of the sirtuin family, failed to inhibit the reduction in H3K14ac (Fig. 2a). In contrast, treatment with trichostatin A (TSA), a pan-inhibitor of the HDAC family, completely prevented this decrease (Fig. 2b), indicating that the classic HDAC family deacetylates H3K14ac during zinc deficiency.

Next, we attempted to identify the specific member of the HDAC family responsible for the deacetylation of H3K14ac during zinc deficiency. However, the knockdown of individual members of the HDAC family did not prevent the zinc-deficient stress-dependent deacetylation of H3K14ac (Fig. 2c). In addition, SAHA, a pan-inhibitor of the HDAC family, but not other subtype-specific HDAC inhibitors (TMP195: HDAC4/5/7/9, tubastatin: HDAC6, UF010: HDAC1/2/3/6/8/10, MS275: HDAC1/2/3/8), effectively inhibited the TPEN-induced deacetylation of H3K14ac (Extended Data Fig. 2a,b). These data suggest that several HDAC family members cooperatively contribute to the deacetylation of H3K14ac during zinc deficiency.

To examine the possibility that zinc-deficient stress enhances the deacetylation activity of the HDAC family towards H3K14ac, we measured HDAC activity employing an *in vitro* HDAC assay using purified histones. The basal HDAC activity for H3K14ac in cell lysates did not differ in the presence and absence of TPEN, suggesting that zinc deficiency in cells enhances the deacetylation of H3K14ac through an independent mechanism that regulates HDAC activity (Fig. 2d). These data indicate that several members of the classic HDAC family are needed to deacetylate H3K14ac during zinc deficiency but are not direct regulatory targets of zinc deficiency.

Loss of KAT7 activity during zinc deficiency

Given that HDAC activity is not enhanced under zinc-deficient conditions, we reasoned that zinc deficiency downregulates the activity of HATs towards H3K14. First, to identify the specific HAT responsible for H3K14ac in HEK293A cells, we performed an siRNA screen using siRNAs targeting 17 human HATs and found that the knockdown of K (lysine) acetyl transferase 7 (KAT7) led to a significant decrease in H3K14ac (Fig. 3a). This decrease was also observed when cells were treated with WM-3835, a specific inhibitor of KAT7[15] (Extended Data Fig. 3a), indicating the crucial role of KAT7 in the acetylation of H3K14. Thus, we focused on the regulatory mechanisms of the KAT7 HAT activity during zinc deficiency.

Previous reports have shown that KAT7 undergoes degradation in response to DNA damage and lipopolysaccharide stimulation via the ubiquitin–proteasome pathway[16,17]. However, our investigation indicated that the effect of TPEN on the protein level of KAT7 was limited (Extended Data Fig. 3b). While treatment with the proteasome inhibitor MG132, but not the autophagy inhibitor Bafilomycin A1, inhibited the slight

TPEN-induced decrease in KAT7, both inhibitors had little effect on the decrease in H3K14ac. These results suggest that the slight TPEN-dependent degradation of KAT7 is not a primary cause of the reduction in H3K14ac during zinc deficiency.

Several reports have demonstrated that KAT7 localizes in the nucleus to acetylates histones[18,19]. We investigated the possibility that the subcellular localization of KAT7 changes during zinc deficiency. However, immunofluorescence analysis of endogenous KAT7 revealed that KAT7 localized in the nucleus after TPEN treatment (Extended Data Fig. 3c), suggesting a change in subcellular localization is not involved in the regulation of KAT7 during zinc deficiency.

Interactome analyses demonstrated that KAT7 forms a multisubunit complex including BRPF1/2/3, JADE1/2/3, ING4/5, and MEAF6[20–26]. Given that these interactors have been reported to directly bind to KAT7 to increase its HAT activity, we hypothesized that zinc deficiency leads to the dissociation of KAT7 from the complex. Systematic knockdown of each interactor revealed that BRPF2 and MEAF6 play a critical role in the acetylation of H3K14 in HEK293A cells (Extended Data Fig. 3d). However, treatment with TPEN did not dissociate KAT7 from each component (Extended Data Fig. 3e). These findings suggest that the disruption of the KAT7 complex is not a cause of the reduction in H3K14ac during zinc deficiency.

Since working hypotheses based on previous reports were not applicable in this case, we next investigated whether zinc deficiency directly affects KAT7 activity by employing an *in vitro* HAT assay. The treatment of cells with TPEN strongly inhibited the HAT activity of immunoprecipitated KAT7 to a similar level as that of the HAT-dead EQ mutant (Fig. 3b). In addition, the KAT7 HAT activity in cells cultured in low-zinc-medium was attenuated in a time-dependent manner, which was followed by the deacetylation of H3K14ac (Fig. 3c). These results suggest that KAT7 loses its enzymatic activity under zinc deficiency.

Zinc coordination in the KAT7 MYST domain regulates HAT activity towards H3K14

KAT7 possesses two zinc finger domains: one is located within the MYST-type HAT domain (MYST domain), and the other is in the N-terminal region (Fig. 3d). We speculated that the loss of zinc coordination during zinc deficiency dysregulates the KAT7 HAT activity. To test this possibility, we examined whether the zinc finger

domains in KAT7 are needed for the KAT7 HAT activity. Depleting *KAT7* using the CRISPR–Cas9 system resulted in the decreased H3K14ac levels in HEK293A cells (Extended Data Fig. 3f). Adding back KAT7 wild-type (WT) or KAT7 mutants with mutations in the N-terminal zinc finger (C185A, C190A, C203A, and C209A) into the *KAT7* knockout HEK293A cell line restored the H3K14ac level (Extended Data Fig. 3f). In contrast, the reintroduction of KAT7 mutants with mutations in the zinc finger within the MYST domain (C368A, C371A, H384A, and C388A) failed to do so. In support of this, immunoprecipitated KAT7 mutants harbouring a zinc finger mutation in the MYST domain showed no HAT activity for H3K14 *in vitro*, while KAT7 mutants with a zinc finger mutation in the N-terminal region had HAT activity similar to that with WT KAT7 (Fig. 3e). These results suggest that the zinc finger within the MYST domain and zinc-binding amino acid residues are needed for the KAT7 HAT activity.

Next, we analysed the properties of recombinant proteins purified from *E. coli*. We tried to obtain full-length KAT7, but were unsuccessful. Thus, we purified the recombinant KAT7 HAT domain (recKAT7^{HAT}), which includes the MYST domain. Consistent with the results above, recKAT7^{HAT} WT, but not the recKAT7^{HAT} EQ mutant or recKAT7^{HAT} C371A mutant, exhibited HAT activity towards H3K14 (Fig. 3f). Notably, the ZnAF-2 assay demonstrated that recKAT7^{HAT} C371A coordinates with substantially less zinc than recKAT7^{HAT} WT (Fig. 3g), suggesting the critical role of proper zinc coordination in the MYST domain for the KAT7 HAT activity.

To further assess the role of zinc in KAT7, we manipulated the zinc metalation status of KAT7 *in vitro* and examined the effect on the HAT activity. First, we attempted to demetallate zinc from KAT7 *in vitro*. However, even when recKAT7^{HAT} WT was treated with TPEN *in vitro*, recKAT7^{HAT} WT still coordinated zinc and showed the HAT activity (Extended Data Fig. 3g,h). Consistent with this, *in vitro* TPEN treatment of KAT7 immunoprecipitated from HEK293A cells did not affect the HAT activity (Extended Data Fig. 3i). These results suggest that KAT7 coordinates zinc much more strongly than TPEN and that it was unsuccessful to demetallate zinc from KAT7 *in vitro*. Next, we examined the effect of *in vitro* zinc repletion. As expected, *in vitro* zinc addition to KAT7 WT immunoprecipitated from HEK293A cells treated with TPEN, but not KAT7 C371A, restored the HAT activity in a dose-dependent manner (Fig. 3h). Collectively, these results suggest that KAT7 loses zinc from the MYST-type zinc

finger domain during zinc deficiency, which leads to the decreased HAT activity towards H3K14.

Loss of H3K14ac on the enhancer induces *ZIP10* expression to maintain cellular zinc homeostasis

Next, we questioned the physiological role of transcriptional changes through the drastic reduction in H3K14ac during zinc deficiency. We and others previously showed that H3K14ac regulates gene expression at promoters and enhancers[27–29]. We speculated that genes responsible for maintaining cellular zinc homeostasis are regulated by H3K14ac. Three gene sets in the Molecular Signatures Database (MSigDB) list genes involved in zinc homeostasis[30,31]. We systematically integrated our gene expression profile data in HeLa cells under zinc deficiency and a publicly available H3K14ac ChIP-seq data from ENCODE[32]. This analysis revealed that multiple genes are transcriptionally altered during zinc deficiency and also have an H3K14ac signal on their promoter or enhancer regions in the basal state (Fig. 4a), suggesting that these genes may be regulated by the reduction in H3K14ac during zinc deficiency. Among these genes, we became interested in the plasma membrane-localized ZIPs, which play a key role in importing zinc from extracellular sources. Quantitative PCR (qPCR) analysis confirmed our microarray data (Fig. 4b). In particular, the notable upregulation of *ZIP10* led us to focus on the physiological role of *ZIP10* upregulation during zinc deficiency.

In HeLa cells, zinc supplementation suppressed the decrease in H3K14ac during zinc deficiency, which is well correlated with the KAT7 HAT activity (Extended Data Fig. 4a, b). Treatment with TSA, a pan-HDAC inhibitor, also suppressed the decrease in H3K14ac, but did not restore the KAT7 HAT activity. Under these experimental conditions, we examined whether zinc-dependent regulation of H3K14ac regulates *ZIP10* expression. Zinc supplementation or TSA treatment counteracted the upregulation of *ZIP10* during zinc deficiency (Fig. 4c). Using a membrane protein biotinylation assay, we confirmed that zinc deficiency led to the expression of ZIP10 at the plasma membrane, which was suppressed by treatment with zinc or TSA (Fig. 4d). In addition, the H3K14ac signal on the enhancer regions of *ZIP10*, which were predicted by EnhancerAtlas 2.0[33], significantly decreased during zinc deficiency, while the signal on the promoter region did not exhibit a decrease (Fig. 4e, left graph,

Extended Data Fig. 4c). This decrease in the enhancer regions was completely suppressed by the treatment with zinc or TSA. Moreover, this decrease in the enhancer region of H3K14ac and increase in *ZIP10* mRNA were also confirmed to be dependent on KAT7 by the knockdown of KAT7 (Fig. 4e, right graph, Extended Data Fig. 4d,e). These results suggest that *ZIP10* expression is regulated by KAT7-catalysed H3K14ac on its enhancer regions.

To investigate whether the *ZIP10* upregulation contributes to maintaining zinc homeostasis, we assessed cellular zinc levels indirectly by measuring *MT2A* mRNA, the expression of which is well known to change depending on the concentration of cellular zinc[34,35]. Consistent with the previous reports, zinc supplementation in cells cultured in a low-zinc medium drastically upregulated *MT2A*, which was suppressed by the knockdown of *ZIP10* (Extended Data Fig. 4f). Notably, only *ZIP10* knockdown, but not the knockdown of other *ZIPs*, significantly attenuated the upregulation of *MT2A* (Extended Data Fig. 4g), suggesting the critical role of ZIP10 in importing zinc during zinc deficiency. To directly assess zinc uptake through ZIP10, we employed ZnDA-3H, a cell-permeable fluorescent Zn^{2+} probe that can be localized to specific subcellular compartments using a HaloTag technology[36]. ZnDA-3H was localized in the cytosol by expressing Halo-NES, and zinc influx was measured under these experimental conditions. As a result, the cells cultured in a low-zinc medium showed a significant increase in the import of zinc ($\Delta [Zn^{2+}] = 80.8 \pm 3.0$ pM) compared to the cells cultured in a normal medium (42.4 ± 4.0 pM) (Fig. 4f). In contrast, TSA treatment suppressed zinc uptake (44.5 ± 8.4 pM), suggesting a critical role of H3K14ac in zinc influx. Remarkably, zinc uptake was significantly inhibited by ZIP10 knockdown (siRNA#1, 18.7 ± 5.3 pM; siRNA#2, 16.2 ± 4.3 pM) compared to the control knockdown (91.9 ± 6.2 pM) (Fig. 4g). Collectively, these data suggest that the zinc influx induced by the addition of zinc to zinc-deficient cells is primarily driven by the H3K14 deacetylation-dependent increase in ZIP10 expression.

Finally, we examined the biological role of the ZIP10 upregulation during zinc deficiency. A previous study showed that zinc deficiency induces cell cycle arrest and that subsequent zinc repletion facilitates cell cycle re-entry[37]. By employing an EdU assay, we confirmed that zinc deficiency indeed arrests the cell cycle and that subsequent zinc supplementation induces cell cycle re-entry (Fig. 4h, siCtrl). Notably, knockdown of ZIP10 inhibited the process of cell cycle re-entry (Fig. 4h, siZIP10#1 and

siZIP10#2). This finding reinforces the importance of ZIP10 upregulation during zinc deficiency in cellular biological processes (Fig. 4i).

Discussion

In this study, we show that zinc deficiency stress is converted to a decrease in H3K14ac. Although we focused on the regulation of H3K14ac-mediated ZIP10 expression, the global decrease in H3K14ac during zinc deficiency reminds us that genes other than ZIP10 should be simultaneously regulated by the decrease in H3K14ac. Indeed, integrated analysis of ChIP-seq data on H3K14ac from public databases and our microarray data suggests that H3K14ac on enhancer regions may be involved in the regulation of multiple genes associated with the cellular responses during zinc deficiency, including *ZIP7*, *ZnT1*, and metallothioneins (*MT1E*, *MT1X*, *MT2A*) (Fig. 4a). ZIP7 is a zinc transporter that localizes in the ER and Golgi apparatus and transports zinc from these organelles into the cytosol[38,39]. It is possible that intracellular zinc transport though ZIP7 cooperatively acts to maintain cytosolic zinc homeostasis. ZnT1 belongs to the Zn transporter (ZnT) family. ZnT1 localizes to the plasma membrane and exports excess cytosolic zinc to the extracellular space[40]. Downregulation of ZnT1 during zinc deficiency helps to maintain cytosolic zinc levels. MT2A is a member of the metallothionein family, which serves as an intracellular zinc reservoir as its expression is downregulated during zinc deficiency[41], which correlates well with our microarray data. Comprehensive analysis of gene regulation mediated by the decrease in H3K14ac during zinc deficiency and its physiological roles awaits future investigation.

We have shown the possibility that H3K14ac regulates the ZIP10 expression via its enhancer regions, but the mechanism remains still unclear. H3K14ac acts as a binding site for numerous bromodomain proteins, as referred to as “readers”[42]. Our results suggest that transcriptional repressive readers may reside in the enhancer regions of ZIP10 at basal state. Several groups, including our laboratory, have reported that bromodomain-containing proteins such as ZMYND8 and BAZ2A recognize H3K14ac on enhancer regions to repress gene transcription[27–29], whereas there are at least 10 readers have been shown to recognize H3K14ac[43]. Identification of the specific reader that recognizes H3K14ac on the enhancer of *ZIP10* is a future challenge.

Regulation of ZIPs on the plasma membrane at the protein level contributes to the maintenance of zinc homeostasis. For example, ZIP4 is degraded via endocytosis under

normal conditions, whereas endocytosis is suppressed during zinc deficiency, leading to an increase in the amount of ZIP4 on the plasma membrane and enhanced zinc influx[44,45]. Another example includes the phosphorylation-dependent regulation of ZIP7 activity[39]. However, little is known about the regulation of ZIP10 at the protein level, except that ZIP10 forms a heteromeric complex with ZIP6[46]. The regulatory mechanisms of ZIP10 at the protein level need to be investigated.

Our study suggests the possibility that zinc-deficient stress leads to loss of zinc coordination in KAT7; however, it remains unclear how zinc is released from KAT7. Although TPEN is a chelator with a high affinity for zinc[47], *in vitro* TPEN treatment did not affect the coordination of zinc or the HAT activity of KAT7 (Extended Data Fig. 3g,h). This result suggests that zinc is tightly coordinated in KAT7, and it is unlikely that zinc is spontaneously released from KAT7 during zinc deficiency. One possible mechanism is that unidentified cellular molecule(s) may recognize the decreased concentration of zinc and facilitate zinc dissociation from KAT7 in the cell. The other possibility is that the activity of certain chaperones that help coordinate zinc in KAT7 may be reduced under zinc-deficient conditions. Recent reports have demonstrated that proper zinc transport mediated by a zinc chaperone regulates the activity of the zinc-dependent enzymes[48,49]. Moreover, *in vitro* zinc repletion of KAT7 WT immunoprecipitated from the cells treated with TPEN did not fully restore the KAT7 HAT activity (Fig. 3h). This raises the possibility that something irreversible other than the loss of zinc coordination, such as changes in the PTMs of KAT7, happens in cells under zinc-deficient conditions. Additional studies are necessary in order to elucidate the precise regulatory mechanism of the KAT7 HAT activity during zinc deficiency.

Although zinc deficiency has been implicated in numerous human diseases, the causal molecular mechanisms remain largely unexplored. This study provides evidence that zinc deficiency is associated with a loss of KAT7 activity, which may advance our understanding of the mechanisms underlying various diseases caused by zinc deficiency. For example, zinc deficiency during pregnancy has devastating effects on the newborn such as growth impairment and low birth weight[50]. From the viewpoint of KAT7, *Kat7* knockout mice show decreased transcription of genes essential for embryonic development due to a global reduction in H3K14ac, which leads to embryonic lethality[51]. This suggests a link between zinc deficiency and the loss of KAT7 activity during embryonic development. Moreover, KAT7 plays key roles in immunity by regulating the

functions and differentiation of T cells[52,53], which was observed in model rodents fed a zinc-deficient diet[54]. Thus, the biological phenomena observed during zinc deficiency will be better understood from the perspective of the functional regulation of KAT7-catalysed H3K14ac.

Materials and Methods

A list of the primers and siRNAs used in this study is provided in Table 1.

Plasmids

The cDNAs encoding human KAT7, BRPF1, BRPF2, BRPF3, JADE1, JADE2, JADE3, ING4, ING5, and MEAF6 were amplified by PCR using KOD One PCR Master Mix -Blue- (TOYOBO, KMM-201) and inserted into pcDNA3/GW with an HA or a FLAG tag (Invitrogen) or into pMAL-c6T (New England Biolabs). The mutated constructs were prepared by PCR-mediated site-directed mutagenesis. A single guide RNA (sgRNA) targeting *KAT7* (5'-AGCCGCCGGCAATGCCGCGA-3') was designed using CHOPCHOP (https://chopchop.cbu.uib.no). The sgRNA was inserted into pX459 (Addgene, 62988).

Cell culture

HEK293A cells, U2OS cells, HCT116 cells, and Neuro2A cells were maintained in high-glucose Dulbecco's modified Eagle's medium (DMEM) (Sigma–Aldrich, D5796; Wako, 044-29765). HeLa cells were maintained in low-glucose DMEM (Wako, 041-29775). Each type of culture medium was supplemented with 10% foetal bovine serum (FBS) (Gibco, 10270-106) and 100 units/ml penicillin G (Meiji Seika, 01028-85). All cell lines were grown in 5% CO_2 at 37°C.

Preparation of zinc-deficient medium

FBS was incubated with Chelex-100 resin (Bio-Rad, 1422832) at a final concentration of 0.05 g/mL at 4°C with rotation. After 12 h, the mixture was centrifuged at 500 × g for 5 min. The supernatant was passed through a Millex-GV 0.22 μM PVDF filter (Millipore, Cat#SLGVR33RS). Cell culture medium supplemented with Chelex-100 resin-treated FBS at a final concentration of 10% was used as zinc-deficient medium.

Transfection

Plasmid transfection was performed using Polyethylenimine"MAX" (Polysciences, 24765) or Lipofectamine 2000 (Thermo Fisher Scientific, 11668019) according to the manufacturer's instructions. siRNA-mediated knockdown was performed using Lipofectamine RNAiMAX (Thermo Fisher Scientific, 13778500) at a final siRNA

concentration of 10 or 20 nM by reverse transfection, according to the manufacturer's instructions.

Generation of knockout cell lines

To generate *KAT7* knockout HEK293A cells or HeLa cells, cells were transfected with pX459 encoding a sgRNA targeting *KAT7*. Forty-eight hours after transfection using Lipofectamine 2000, the cells were selected by 1.0 µg/mL puromycin (Gibco, A11138-03) treatment for another 48 h. The selection medium was replaced with fresh standard medium, and the cells were grown for 3 days. Limiting dilution was performed to obtain single-cell clones. The knockout status of the clones was confirmed by immunoblotting.

Immunoblotting

Cells were lysed in a cell lysis buffer (20 mM Tris-HCl pH 7.5, 150 mM NaCl, 10 mM EDTA, 1% Triton X-100, 5 µg/mL leupeptin, 1 mM phenylmethylsulfonyl fluoride (PMSF) and 2 nM TSA) for 10 min at 4°C. The lysates were sonicated with 2 sets of 10-sec pulses using an ultrasonic homogenizer (SMT, UH-50). The cell debris was cleared by centrifugation at 17,700 × g for 15 min. The supernatant was mixed with a sample buffer (80 mM Tris-HCl pH 8.8, 80 µg/mL bromophenol blue, 28.8% glycerol, and 4% SDS) supplemented with 10 mM DTT and incubated for 3 min at 98°C. The samples were then resolved by SDS–PAGE and transferred onto Immobilon-P PVDF membranes (Millipore, IPVH00010). Blocking was performed with 5% skim milk (Megmilk Snow Brand) in TBS-T (50 mM Tris-HCl pH 8.0, 150 mM NaCl and 0.05% Tween 20) for 30 min at room temperature. After incubation of the membranes with the indicated primary antibodies for 12-36 hours at 4°C and corresponding HRP-linked secondary antibodies for 1-2 hours at room temperature, the chemiluminescent signals enhanced by ECL Select (Cytiva, RPN2235) were detected using a Fusion Solo 7S instrument (M&S Instruments). Quantification of the bands was performed using Fiji software[55].

Coimmunoprecipitation analysis

Cell lysates were incubated with anti-DYKDDDDK-tagged antibody beads (Wako, 016-22784) at 4°C for 10 min. The beads were washed with washing buffer 1 (20 mM Tris-HCl pH 7.5, 500 mM NaCl, 5 mM EGTA and 1% Triton X-100) and washing

buffer 2 (20 mM Tris-HCl pH 7.5, 150 mM NaCl and 5 mM EGTA). The washed beads were mixed with sample buffer (80 mM Tris-HCl pH 8.8, 80 μg/mL bromophenol blue, 28.8% glycerol, and 4% SDS) supplemented with 20 mM DTT for 5 min at room temperature and then incubated for 3 min at 98°C. The samples were separated by SDS–PAGE and immunoblotted with antibodies.

Immunofluorescence analysis

For confocal microscopy, cells were grown on glass coverslips (Matsunami Glass, C015001). For imaging with a high-content imaging system, cells were grown on a 96-well plate (Corning, 353072). The cells were fixed with 4% paraformaldehyde in PBS for 10 min and permeabilized with 0.2% Triton X-100 in PBS for 5 min. After blocking with 1% BSA (Iwai Chemicals, A001) in TBS-T for 1 h, the cells were incubated with the indicated primary antibodies overnight at 4°C. After washing three times with PBS, the cells were incubated with fluorophore-conjugated secondary antibodies at room temperature for 2 h and then with Hoechst 33342 (Dojindo, 346-07951) for 20 min. After washing three times with PBS, the cells were mounted with Fluoromount (Diagnostic BioSystems, K024) for confocal microscopy. Images were acquired using an LSM880 with Airyscan (Zeiss) with a 63×/1.40 oil immersion objective or a CellInsight NXT HCS system (Thermo Scientific). The contrast and brightness of the images were adjusted using Fiji software. Quantification of the images was performed using Fiji software or CellProfiler[56].

Histone extraction

Purified histones for the *in vitro* HDAC assay and *in vitro* HAT assay were obtained by the acid-extraction method as previously described[57]. Briefly, HEK293A cells or HEK293A *KAT7* KO cells were incubated in hypotonic lysis buffer for 30 min at 4°C with rotation. After centrifugation at 10,000 × g for 10 min at 4°C, the cell pellets were resuspended in 0.4 N H_2SO_4 and incubated for 30 min at 4°C with rotation. After centrifugation at 15,100 × g for 10 min at 4°C, the supernatant was transferred to a fresh 1.5 mL tube. Then, trichloroacetic acid (TCA) was added to the supernatant dropwise and incubated for 30 min on ice. After centrifugation at 15,100 × g for 10 min at 4°C, the pelleted histones were washed twice with ice-cold acetone. The pellet histones were air-dried at room temperature and dissolved in TBS at a final concentration of 3 μg/μL.

***In vitro* HDAC assay**

HEK293A cells treated with DMSO or 10 μM TPEN for 1 h or 2 h were lysed in a cell lysis buffer for *in vitro* HDAC assay (20 mM Tris-HCl pH 7.5, 150 mM NaCl, 10 mM EDTA, 1% Triton X-100, 5 μg/mL leupeptin, and 1 mM PMSF) for 10 min at 4°C. Purified histones were mixed with the cell lysates and incubated at 37°C for 0.5, 1 or 2 h with DMSO or 10 nM TSA. Then, the samples were mixed with an equal volume of 2x sample buffer supplemented with 10 mM DTT and incubated for 3 min at 98°C, followed by SDS–PAGE and immunoblotting.

***In vitro* HAT assay**

To measure the activity of KAT7 immunoprecipitated from cells, HEK293A cells transfected with FLAG-KAT7 WT or mutants were lysed in cell lysis buffer for an *in vitro* HAT assay (20 mM Tris-HCl pH 7.5, 150 mM NaCl, 10 mM EDTA, 1% Triton X-100, 5 μg/mL leupeptin, and 1 mM PMSF). The cell lysates were incubated with anti-FLAG M2-agarose gel (Sigma–Aldrich, A2220) at 4°C for 5 min. The beads were washed twice with washing buffer 3 (20 mM Tris-HCl pH 7.5, 150 mM NaCl, 1% Triton X-100) and once with TBS. Purified histones at a final concentration of 0.5 μM were mixed with the beads and with 50 μM acetyl-CoA in TBS and incubated for 30 min at 30°C with frequent mixing (1,200 rpm) using a Thermomixer C (Eppendorf). The samples were mixed with an equal volume of 2x sample buffer supplemented with 10 mM DTT and incubated for 3 min at 98°C, followed by SDS–PAGE and immunoblotting. To measure the activity of the recombinant KAT7 HAT domain, 5 μM recombinant protein was used.

Recombinant protein purification

The KAT7 HAT domain (a.a. 336-611) WT or C371A mutants encoded in pMAL-c6T were expressed in *E. coli* BL21 cells. Expression was induced by incubation in LB medium supplemented with 0.3 mM IPTG at 25°C for 1.5 h. The cells were pelleted and resuspended in PBS supplemented with 1% Triton X-100 and 1 mM PMSF. After sonication with 4 sets of 30-sec pulses using an ultrasonic homogenizer, the cell debris was cleared by centrifugation at 26,800 × g for 30 min. The supernatants were incubated with Ni Sepharose 6 Fast Flow (Cytiva, 17531806) at 4°C for 8 h. The beads

were then washed twice with PBS and twice with TBS and eluted with a 250 mM imidazole solution in TBS using Poly-Prep Chromatography Columns (Bio-Rad, 7311550). The eluates were loaded onto a Superose 6 Increase 10/300 GL column on an AKTA purifier (GE Healthcare) and dialyzed in TBS overnight at 4°C. The purity and concentration of the final products were estimated by Coomassie blue staining of SDS–PAGE gels.

qPCR analysis

Total RNA was isolated from cells using Isogen (Nippongene, 319-90211) and reverse transcribed with ReverTra Ace qPCR RT Master Mix with gDNA Remover (TOYOBO, FSQ-301) according to the manufacturer's instructions. Samples of the qPCR mixture were prepared using the KAPA SYBR Fast qPCR Kit (Kapa Biosystems, KK4602). qPCR was then performed on a LightCycler 96 (Roche) or QuantStudio 1 (Thermo Fisher Scientific) instrument. Data for each mRNA were normalized to that of RPS18.

ChIP–qPCR

Chromatin samples for ChIP–qPCR were prepared using a SimpleChIP Enzymatic Chromatin IP Kit (Cell Signaling Technology, 9003) according to the manufacturer's instructions. The chromatin samples were incubated with anti-H3K14ac antibody (Abcam, ab52946) or anti-histone H3 antibody (Cell Signaling Technology, 4499) at 4°C for 8 h with rotation. Then, the samples were incubated with Dynabeads Protein G (VERITAS, DB10004) at 4°C for 2 h with rotation. After washing three times with low-salt buffer (1% SDS, 1% Triton-X, 2 mM EDTA, 20 mM Tris-HCl pH 8.0 and 150 mM NaCl) and once with high-salt buffer (1% SDS, 1% Triton-X, 2 mM EDTA, 20 mM Tris-HCl pH 8.0 and 500 mM NaCl), the chromatin was eluted with elution buffer (1% SDS, 10 mM EDTA and 50 mM Tris-HCl pH 8.0) for 30 min at 65°C with frequent mixing (1,200 rpm) using a Thermomixer C. The purified DNA was analysed as described in the "qPCR analysis" section. ChIP-seq data used for designing primers were downloaded from the ENCODE portal[58] with the following identifier: ENCFF002QJL. Data visualization was performed with Integrative Genomics Viewer (Broad Institute).

ZnAF2 assay

Recombinant proteins or $ZnCl_2$ solution for normalization was incubated with 10 μM ZnAF-2 (Goryo Chemical, SK2001-01) in TBS for 30 min at room temperature. The fluorescence signal was detected with a Varioskan microplate reader (Ex/Em = 492/515 nm, Thermo Scientific).

ERSE sequence analysis

ERSE sequences, CCAAT-$(N)_9$-CCAC[A/G], on the human genome GRCh/hg38 were retrieved from the GGGenome ultrafast sequence search browser. Among the sequences obtained (plus strand, 3764 sequences; minus strand, 3874 sequences), 1897 sequences were annotated as sequences on gene promoters by employing HOMER. The number of ERSE sequences on genes that were upregulated during zinc deficiency was counted programmatically. Gene expression profile data analysed by GEO2R were downloaded from the GEO repository (GSE49657, GSE99204, GSE108923, and GSE135873). Genes with a fold change in expression greater than 2 were considered upregulated.

ChIP-seq data analysis

The H3K14ac signals on the promoters and enhancers were calculated programmatically. The promoter region was defined as the region 5000 bp upstream and 1000 bp downstream from the transcription start site (TSS). A BED file of 5,000 bp upstream of the tentative TSS was retrieved from the UCSC Genome browser database. The region 1000 bp downstream from the TSS was obtained by bedtools. BED files for enhancer regions were downloaded from the EnhancerAtlas2.0[33] and FANTOM5[59,60] database. A BigWig file for H3K14ac was downloaded from ENCODE (ENCFF002QJL). The H3K14ac signals on the promoter regions and the enhancer regions were analysed by wigglescout, an R package (https://github.com/cnluzon/wigglescout/) on the super computer SHIROKANE. The super-computing resource was provided by Human Genome Center (the Univ. of Tokyo).

EdU assay

HeLa cells were grown on a 96-well plate and analysed with a Click-iT EdU imaging kit (Invitrogen, C10340). The cells were incubated with 10 μM EdU for 1 h, fixed with 4% paraformaldehyde in PBS for 15 min at room temperature, and washed twice with PBS

containing 3% BSA. The cells were permeabilized with 0.5% Triton X-100 in PBS for 20 min at room temperature and washed twice with PBS containing 3% BSA. Then, Click-iT reaction cocktail was added and allowed to react for 30 min at room temperature. After washing twice with PBS containing 3% BSA, the cells were incubated with Hoechst 33342 (1:2000) in PBS for 30 min at room temperature. Images were acquired with a CellInsight NXT automated microscope and analysed with CellProfiler.

Membrane protein biotinylation assay

Cells were incubated with 0.4 mg/mL biotin (EZ-Link Sulfo-NHS-SS-Biotin, Thermo Fisher Scientific, 21331) in PBS(+) (PBS containing 50 mM $MgCl_2$ and 100 mM $CaCl_2$) and washed twice with 150 mM glycine in PBS(+). Cells were lysed as described in the "Immunoblotting" section. The cell lysates were pulled down with streptavidin agarose resin (Thermo Fisher Scientific, 20353). The resin samples were washed twice with washing buffer 1 and once with washing buffer 2. The samples were subjected to immunoblotting.

Zinc imaging by ZnDA-3H

Zinc measurement with ZnDA-3H was performed as described previously with minor optimization[36,61]. HeLa cells were reverse-transfected with 10 μM siRNA. The cells were then transfected with Halo-NES and cultured for 24 hours. The cells were replated on 35 mmφ glass bottom dishes (Matsunami, D11130H) that were coated with 1% Cellmatrix Type I-C (Nitta Gelatin, KP-4100). After 24 hours, the cells were incubated with zinc-normal medium or zinc-deficient medium for an additional 48 hours. Cells were washed with Chelex-treated HEPES-buffered HBSS (30 mM HEPES-NaOH, pH 7.4, 5.36 mM KCl, 137 mM NaCl), and incubated with serum-free DMEM containing 250 nM ZnDA-3H and 5 nM HTL-TMR for 30 min. After labelling, the cells were incubated for an additional 30 minutes. After incubation, the cells were washed twice with Chelex-treated HEPES-buffered HBSS, and the medium was exchanged for Chelex-treated HBSS buffer. Multichannel time-lapse images were acquired with 4 averages per frame in 30-second intervals. ZnDA-3H or Halo-TMR was excited at 488 nm with an argon laser or at 561 nm with a DPSS laser and detected by a HyD detector (Leica). Images were acquired for 5 minutes, and then the cells were incubated with Chelex-treated HBSS containing 10 μM $ZnCl_2$ for an additional 10 minutes. To obtain additional

images under zinc-deprived and zinc-saturated conditions, the cells were incubated with Chelex-treated HBSS containing 10 μM TPEN for 5 minutes, and then, the cells were incubated with Chelex-treated HBSS containing 400 μM $ZnCl_2$ and 2.0 μM zinc pyrithione for an additional 10 minutes. For presentation, the pseudocolour fluorescence ratio images of ZnDA-3H/HTL-TMR were generated using Fiji software. For quantification of the intensity, we used CellProfiler.

Quantification and statistical analysis

All statistical data were calculated using R (ver. 4.0.5) with RStudio (ver. 2022.12.0+353). P values < 0.05 were considered to indicate statistical significance. Detailed statistical information for each experiment, including the number of biological replicates (n), is shown in the figures and corresponding legends.

Author contributions

Conceptualization, T.F.;

Methodology, T.F, T.K., T.M., and S.M.;

Investigation, T.F., S.T., and L.M.;

Formal analysis, T.F.;

Visualization, T.F. and S.T.;

Funding acquisition, T.F. and H.I.;

Supervision, T.F. and H.I.;

Writing – Original Draft, T.F.;

Writing – Review & Editing, S.T., L.M., T.K., T.M., S.M., I.N., and H.I.

Disclosure and competing interests statement

The authors declare that they have no conflicts of interest.

Code availability

The code used in this study is freely available on GitHub. (https://github.com/FujisawaGroup/).

Acknowledgements

We thank all members and ex-members of the Laboratory of Cell Signaling for fruitful discussions. We are grateful to Dr. Amagai, Y (Tohoku University) for helpful discussions, particularly on zinc imaging. This study was supported by the Japan Agency for Medical Research and Development (AMED) for the Project for Elucidating and Controlling Mechanisms of Aging and Longevity (grant number JP21gm5010001 to H.I.), by the Japan Society for the Promotion of Science (JSPS) for the Grants-in-Aid for Scientific Research (KAKENHI; grant numbers JP22K06610 to T.F. and JP21H04760 to H.I.) and the Grant-in-Aid for Scientific Research on Innovative Areas (KAKENHI; grant number JP22H04804 to T.F.), by the Japan Science and Technology Agency (JST) for Moonshot R&D–MILLENNIA Program (grant number JPMJMS2022-18 to H.I.).

References

1. Andreini, C. & Bertini, I. A bioinformatics view of zinc enzymes. *J. Inorg. Biochem.* **111**, 150–156 (2012).
2. Prasad, A. S. Impact of the discovery of human zinc deficiency on health. *J. Trace Elem. Med. Biol.* **28**, 357–363 (2014).
3. Prasad, A. S., Halsted, J. A. & Nadimi, M. Syndrome of iron deficiency anemia, hepatosplenomegaly, hypogonadism, dwarfism and geophagia. *Am. J. Med.* **31**, 532–546 (1961).
4. Prasad, A. S., Miale, A., Jr & Farid, Z. Zinc metabolism in patients with the syndrome of iron deficiency anemia, hepatosplenomegaly, dwarfism, and hypogonadism. *Journal of Laboratory* (1963).
5. Hara, T. *et al.* Physiological roles of zinc transporters: molecular and genetic importance in zinc homeostasis. *J. Physiol. Sci.* **67**, 283–301 (2017).
6. Kambe, T., Tsuji, T., Hashimoto, A. & Itsumura, N. The Physiological, Biochemical, and Molecular Roles of Zinc Transporters in Zinc Homeostasis and Metabolism. *Physiol. Rev.* **95**, 749–784 (2015).
7. Homma, K. *et al.* SOD1 as a molecular switch for initiating the homeostatic ER stress response under zinc deficiency. *Mol. Cell* **52**, 75–86 (2013).
8. Lichten, L. A., Ryu, M.-S., Guo, L., Embury, J. & Cousins, R. J. MTF-1-mediated repression of the zinc transporter Zip10 is alleviated by zinc restriction. *PLoS One* **6**, e21526 (2011).
9. Millán-Zambrano, G., Burton, A., Bannister, A. J. & Schneider, R. Histone post-translational modifications - cause and consequence of genome function. *Nat. Rev. Genet.* **23**, 563–580 (2022).
10. Brito, S., Lee, M.-G., Bin, B.-H. & Lee, J.-S. Zinc and Its Transporters in Epigenetics. *Mol. Cells* **43**, 323–330 (2020).
11. Richardson, C. E. R. *et al.* A Method for Selective Depletion of Zn(II) Ions from Complex Biological Media and Evaluation of Cellular Consequences of Zn(II) Deficiency. *J. Am. Chem. Soc.* **140**, 2413–2416 (2018).
12. Bin, B.-H. *et al.* Requirement of zinc transporter ZIP10 for epidermal development: Implication of the ZIP10-p63 axis in epithelial homeostasis. *Proc. Natl. Acad. Sci. U. S. A.* **114**, 12243–12248 (2017).

13. Kar, M. *et al.* Zinc Chelation Specifically Inhibits Early Stages of Dengue Virus Replication by Activation of NF-κB and Induction of Antiviral Response in Epithelial Cells. *Front. Immunol.* **10**, 2347 (2019).
14. Yoshida, H., Haze, K., Yanagi, H., Yura, T. & Mori, K. Identification of the cis-Acting Endoplasmic Reticulum Stress Response Element Responsible for Transcriptional Induction of Mammalian Glucose-regulated Proteins: INVOLVEMENT OF BASIC LEUCINE ZIPPER TRANSCRIPTION FACTORS*. *J. Biol. Chem.* **273**, 33741–33749 (1998).
15. MacPherson, L. *et al.* HBO1 is required for the maintenance of leukaemia stem cells. *Nature* **577**, 266–270 (2020).
16. Matsunuma, R. *et al.* UV Damage-Induced Phosphorylation of HBO1 Triggers CRL4DDB2-Mediated Degradation To Regulate Cell Proliferation. *Mol. Cell. Biol.* **36**, 394–406 (2016).
17. Zou, C. *et al.* SCF(Fbxw15) mediates histone acetyltransferase binding to origin recognition complex (HBO1) ubiquitin-proteasomal degradation to regulate cell proliferation. *J. Biol. Chem.* **288**, 6306–6316 (2013).
18. Niida, H. *et al.* Phosphorylated HBO1 at UV irradiated sites is essential for nucleotide excision repair. *Nat. Commun.* **8**, 16102 (2017).
19. Wang, W. *et al.* A genome-wide CRISPR-based screen identifies KAT7 as a driver of cellular senescence. *Sci. Transl. Med.* **13**, (2021).
20. Yan, K. *et al.* Mutations in the Chromatin Regulator Gene BRPF1 Cause Syndromic Intellectual Disability and Deficient Histone Acetylation. *Am. J. Hum. Genet.* **100**, 91–104 (2017).
21. Lalonde, M.-E. *et al.* Exchange of associated factors directs a switch in HBO1 acetyltransferase histone tail specificity. *Genes Dev.* **27**, 2009–2024 (2013).
22. Feng, Y. *et al.* BRPF3-HBO1 regulates replication origin activation and histone H3K14 acetylation. *EMBO J.* **35**, 176–192 (2016).
23. Foy, R. L. *et al.* Role of Jade-1 in the histone acetyltransferase (HAT) HBO1 complex. *J. Biol. Chem.* **283**, 28817–28826 (2008).
24. Xiao, Y. *et al.* HBO1 is a versatile histone acyltransferase critical for promoter histone acylations. *Nucleic Acids Res.* **49**, 8037–8059 (2021).
25. Doyon, Y. *et al.* ING tumor suppressor proteins are critical regulators of chromatin acetylation required for genome expression and perpetuation. *Mol. Cell* **21**, 51–64 (2006).

26. Matsuura, K. *et al.* MEAF6 is essential for cell proliferation and plays a role in the assembly of KAT7 complexes. *Exp. Cell Res.* **396**, 112279 (2020).
27. Savitsky, P. *et al.* Multivalent Histone and DNA Engagement by a PHD/BRD/PWWP Triple Reader Cassette Recruits ZMYND8 to K14ac-Rich Chromatin. *Cell Rep.* **17**, 2724–2737 (2016).
28. Peña-Hernández, R. *et al.* BAZ2A-mediated repression via H3K14ac-marked enhancers promotes prostate cancer stem cells. *EMBO Rep.* **22**, e53014 (2021).
29. Shen, H. *et al.* Suppression of Enhancer Overactivation by a RACK7-Histone Demethylase Complex. *Cell* **165**, 331–342 (2016).
30. Subramanian, A. *et al.* Gene set enrichment analysis: a knowledge-based approach for interpreting genome-wide expression profiles. *Proc. Natl. Acad. Sci. U. S. A.* **102**, 15545–15550 (2005).
31. Liberzon, A. *et al.* Molecular signatures database (MSigDB) 3.0. *Bioinformatics* **27**, 1739–1740 (2011).
32. ENCODE Project Consortium. An integrated encyclopedia of DNA elements in the human genome. *Nature* **489**, 57–74 (2012).
33. Gao, T. & Qian, J. EnhancerAtlas 2.0: an updated resource with enhancer annotation in 586 tissue/cell types across nine species. *Nucleic Acids Res.* **48**, D58–D64 (2020).
34. Heuchel, R. *et al.* The transcription factor MTF-1 is essential for basal and heavy metal-induced metallothionein gene expression. *EMBO J.* **13**, 2870–2875 (1994).
35. Hennigar, S. R. *et al.* Sensitivity and reliability of zinc transporter and metallothionein gene expression in peripheral blood mononuclear cells as indicators of zinc status: responses to ex vivo zinc exposure and habitual zinc intake in humans. *Br. J. Nutr.* **125**, 361–368 (2021).
36. Liu, R. *et al.* Organelle-Level Labile Zn2+ Mapping Based on Targetable Fluorescent Sensors. *ACS Sens* **7**, 748–757 (2022).
37. Lo, M. N., Damon, L. J., Wei Tay, J., Jia, S. & Palmer, A. E. Single cell analysis reveals multiple requirements for zinc in the mammalian cell cycle. *Elife* **9**, (2020).
38. Huang, L., Kirschke, C. P., Zhang, Y. & Yu, Y. Y. The ZIP7 gene (Slc39a7) encodes a zinc transporter involved in zinc homeostasis of the Golgi apparatus. *J. Biol. Chem.* **280**, 15456–15463 (2005).

39. Taylor, K. M., Hiscox, S., Nicholson, R. I., Hogstrand, C. & Kille, P. Protein kinase CK2 triggers cytosolic zinc signaling pathways by phosphorylation of zinc channel ZIP7. *Sci. Signal.* **5**, ra11 (2012).
40. Palmiter, R. D. & Findley, S. D. Cloning and functional characterization of a mammalian zinc transporter that confers resistance to zinc. *EMBO J.* **14**, 639–649 (1995).
41. Kelly, E. J., Quaife, C. J., Froelick, G. J. & Palmiter, R. D. Metallothionein I and II protect against zinc deficiency and zinc toxicity in mice. *J. Nutr.* **126**, 1782–1790 (1996).
42. Fujisawa, T. & Filippakopoulos, P. Functions of bromodomain-containing proteins and their roles in homeostasis and cancer. *Nat. Rev. Mol. Cell Biol.* **18**, 246–262 (2017).
43. Filippakopoulos, P. *et al.* Histone recognition and large-scale structural analysis of the human bromodomain family. *Cell* **149**, 214–231 (2012).
44. Kim, B.-E. *et al.* Zn2+-stimulated endocytosis of the mZIP4 zinc transporter regulates its location at the plasma membrane. *J. Biol. Chem.* **279**, 4523–4530 (2004).
45. Mao, X., Kim, B.-E., Wang, F., Eide, D. J. & Petris, M. J. A histidine-rich cluster mediates the ubiquitination and degradation of the human zinc transporter, hZIP4, and protects against zinc cytotoxicity. *J. Biol. Chem.* **282**, 6992–7000 (2007).
46. Taylor, K. M. *et al.* Zinc transporter ZIP10 forms a heteromer with ZIP6 which regulates embryonic development and cell migration. *Biochem. J* **473**, 2531–2544 (2016).
47. NIST46 | NIST. (2013).
48. Chen, Y.-Y. & O'Halloran, T. V. A zinc chaperone mediates the flow of an inorganic commodity to an important cellular client. *Cell* vol. 185 2013–2015 (2022).
49. Pasquini, M. *et al.* Zng1 is a GTP-dependent zinc transferase needed for activation of methionine aminopeptidase. *Cell Rep.* **39**, 110834 (2022).
50. Scholl, T. O., Hediger, M. L., Schall, J. I., Fischer, R. L. & Khoo, C. S. Low zinc intake during pregnancy: its association with preterm and very preterm delivery. *Am. J. Epidemiol.* **137**, 1115–1124 (1993).
51. Kueh, A. J., Dixon, M. P., Voss, A. K. & Thomas, T. HBO1 is required for H3K14 acetylation and normal transcriptional activity during embryonic development. *Mol. Cell. Biol.* **31**, 845–860 (2011).
52. Newman, D. M., Voss, A. K., Thomas, T. & Allan, R. S. Essential role for the histone acetyltransferase KAT7 in T cell development, fitness, and survival. *J. Leukoc. Biol.* **101**, 887–892 (2017).

53. Heinlein, M. *et al.* The acetyltransferase KAT7 is required for thymic epithelial cell expansion, expression of AIRE target genes, and thymic tolerance. *Sci Immunol* **7**, eabb6032 (2022).
54. Blewett, H. J. & Taylor, C. G. Dietary zinc deficiency in rodents: effects on T-cell development, maturation and phenotypes. *Nutrients* **4**, 449–466 (2012).
55. Schindelin, J. *et al.* Fiji: an open-source platform for biological-image analysis. *Nat. Methods* **9**, 676–682 (2012).
56. Stirling, D. R. *et al.* CellProfiler 4: improvements in speed, utility and usability. *BMC Bioinformatics* **22**, 433 (2021).
57. Shechter, D., Dormann, H. L., Allis, C. D. & Hake, S. B. Extraction, purification and analysis of histones. *Nat. Protoc.* **2**, 1445–1457 (2007).
58. Sloan, C. A. *et al.* ENCODE data at the ENCODE portal. *Nucleic Acids Res.* **44**, D726-32 (2016).
59. Abugessaisa, I. *et al.* FANTOM enters 20th year: expansion of transcriptomic atlases and functional annotation of non-coding RNAs. *Nucleic Acids Res.* **49**, D892–D898 (2021).
60. Lizio, M. *et al.* Gateways to the FANTOM5 promoter level mammalian expression atlas. *Genome Biol.* **16**, 22 (2015).
61. Kowada, T., Watanabe, T., Liu, R. & Mizukami, S. Protocol for synthesis and use of a turn-on fluorescent probe for quantifying labile Zn2+ in the Golgi apparatus in live cells. *STAR Protoc* **2**, 100395 (2021).

Fig. 1

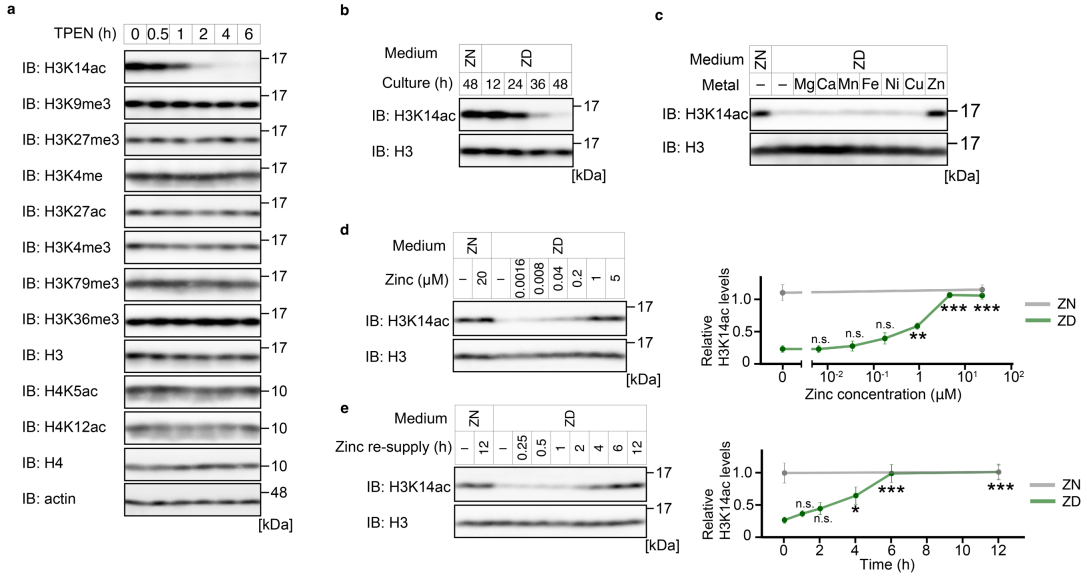
a
TPEN (h) 0 0.5 1 2 4 6
IB: H3K14ac 17
IB: H3K9me3 17
IB: H3K27me3 17
IB: H3K4me 17
IB: H3K27ac 17
IB: H3K4me3 17
IB: H3K79me3 17
IB: H3K36me3 17
IB: H3 17
IB: H4K5ac 10
IB: H4K12ac 10
IB: H4 10
IB: actin 48
[kDa]
b
Medium ZN ZD
Culture (h) 48 12 24 36 48
IB: H3K14ac 17
IB: H3 17
[kDa]
c
Medium ZN ZD
Metal – – Mg Ca Mn Fe Ni Cu Zn
IB: H3K14ac 17
IB: H3 17
[kDa]
d
Medium ZN ZD
Zinc (μM) – 20 – 0.0016 0.008 0.04 0.2 1 5
IB: H3K14ac 17
IB: H3 17
[kDa]
Relative H3K14ac levels
1.0
0.5
0
n.s.
n.s.
n.s.
**
***
***
0
10-2
10-1
1
101
102
Zinc concentration (μM)
ZN
ZD
e
Medium ZN ZD
Zinc re-supply (h) – 12 – 0.25 0.5 1 2 4 6 12
IB: H3K14ac 17
IB: H3 17
[kDa]
Relative H3K14ac levels
1.0
0.5
0
n.s.
n.s.
*
***
***
0 2 4 6 8 10 12
Time (h)
ZN
ZD

Fig. 2

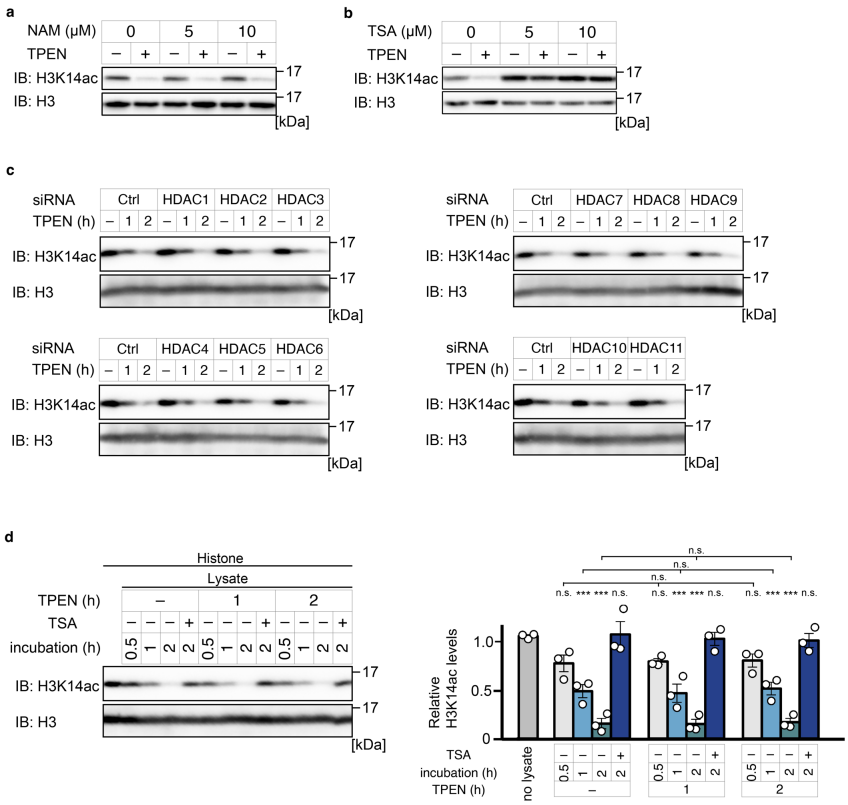
a
NAM (μM) 0 5 10
TPEN – + – + – +
IB: H3K14ac 17
IB: H3 17
[kDa]
b
TSA (μM) 0 5 10
TPEN – + – + – +
IB: H3K14ac 17
IB: H3 17
[kDa]
c
siRNA Ctrl HDAC1 HDAC2 HDAC3
TPEN (h) – 1 2 – 1 2 – 1 2 – 1 2
IB: H3K14ac 17
IB: H3 17
[kDa]
siRNA Ctrl HDAC7 HDAC8 HDAC9
TPEN (h) – 1 2 – 1 2 – 1 2 – 1 2
IB: H3K14ac 17
IB: H3 17
[kDa]
siRNA Ctrl HDAC4 HDAC5 HDAC6
TPEN (h) – 1 2 – 1 2 – 1 2 – 1 2
IB: H3K14ac 17
IB: H3 17
[kDa]
siRNA Ctrl HDAC10 HDAC11
TPEN (h) – 1 2 – 1 2 – 1 2
IB: H3K14ac 17
IB: H3 17
[kDa]
d
Histone
Lysate
TPEN (h) – 1 2
TSA – – – + – – – + – – – +
incubation (h) 0.5 1 2 2 0.5 1 2 2 0.5 1 2 2
IB: H3K14ac 17
IB: H3 17
[kDa]
n.s.
n.s.
n.s.
n.s. *** *** n.s. n.s. *** *** n.s. n.s. *** *** n.s.
Relative H3K14ac levels
1.0
0.5
0
TSA
incubation (h)
TPEN (h)
no lysate
0.5 1 2 2
–
0.5 1 2 2
1
0.5 1 2 2
2

Fig. 3

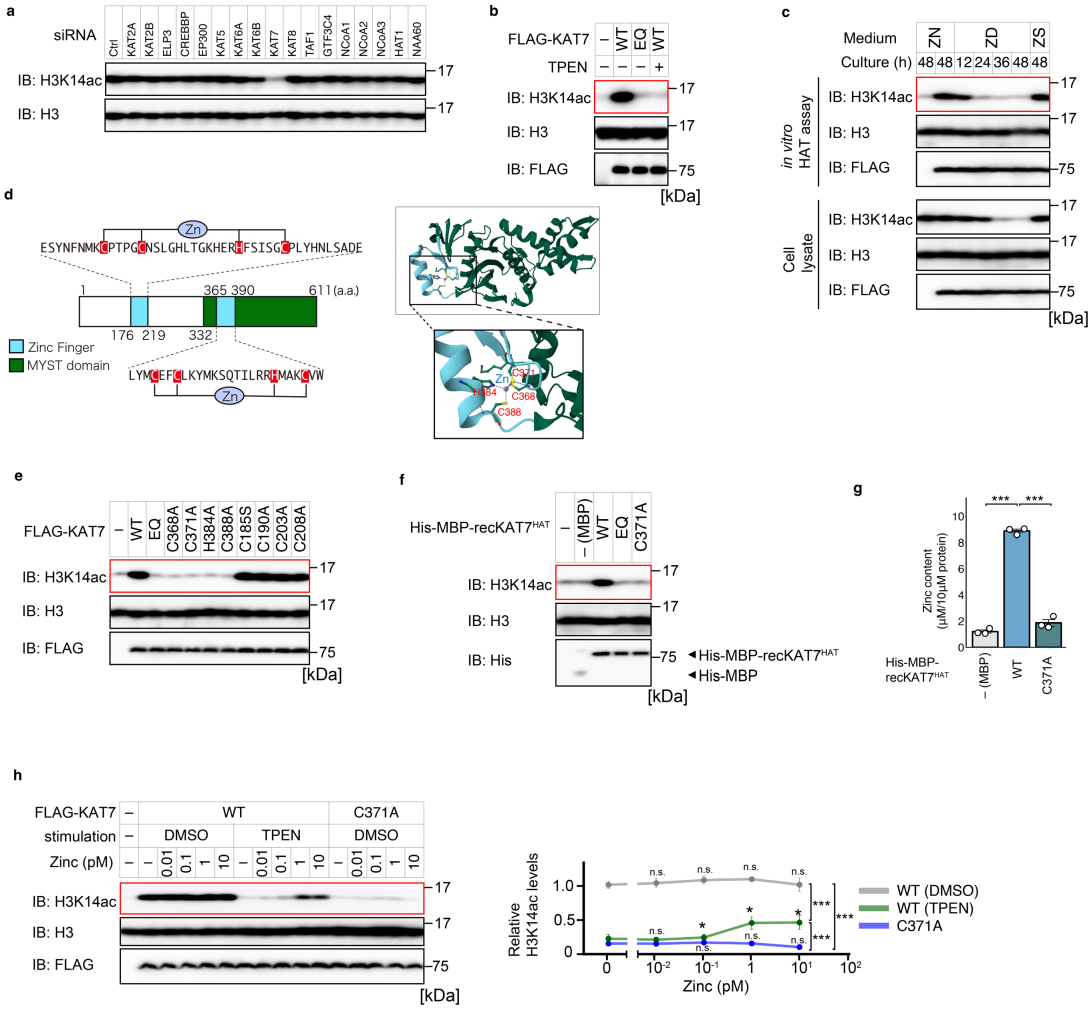
a
siRNA
Ctrl
KAT2A
KAT2B
ELP3
CREBBP
EP300
KAT5
KAT6A
KAT6B
KAT7
KAT8
TAF1
GTF3C4
NCoA1
NCoA2
NCoA3
HAT1
NAA60
IB: H3K14ac
IB: H3
17
b
FLAG-KAT7
TPEN
IB: H3K14ac
IB: H3
IB: FLAG
75
[kDa]
c
Medium
Culture (h)
ZN
ZD
ZS
in vitro HAT assay
Cell lysate
d
Zn
ESYNFNMKCPTPGCNSLGHLTGKHERHFSISGCPLYHNLSADE
1
365 390
611(a.a.)
176 219
332
Zinc Finger
MYST domain
LYMCEFCLKYMKSQTILRRHMAKCVW
C371
H384
C368
C388
e
FLAG-KAT7
WT
EQ
C368A
C371A
H384A
C388A
C185S
C190A
C203A
C208A
f
His-MBP-recKAT7HAT
(MBP)
IB: His
His-MBP-recKAT7HAT
His-MBP
g
Zinc content (μM/10μM protein)
His-MBP-recKAT7HAT
***

h

FLAG-KAT7
stimulation
DMSO
TPEN
Zinc (pM)
0.01
0.1
1
10
C371A
IB: H3K14ac
IB: H3
IB: FLAG
17
75
[kDa]
Relative H3K14ac levels
n.s.
*
***
Zinc (pM)
WT (DMSO)
WT (TPEN)
C371A

Fig. 4

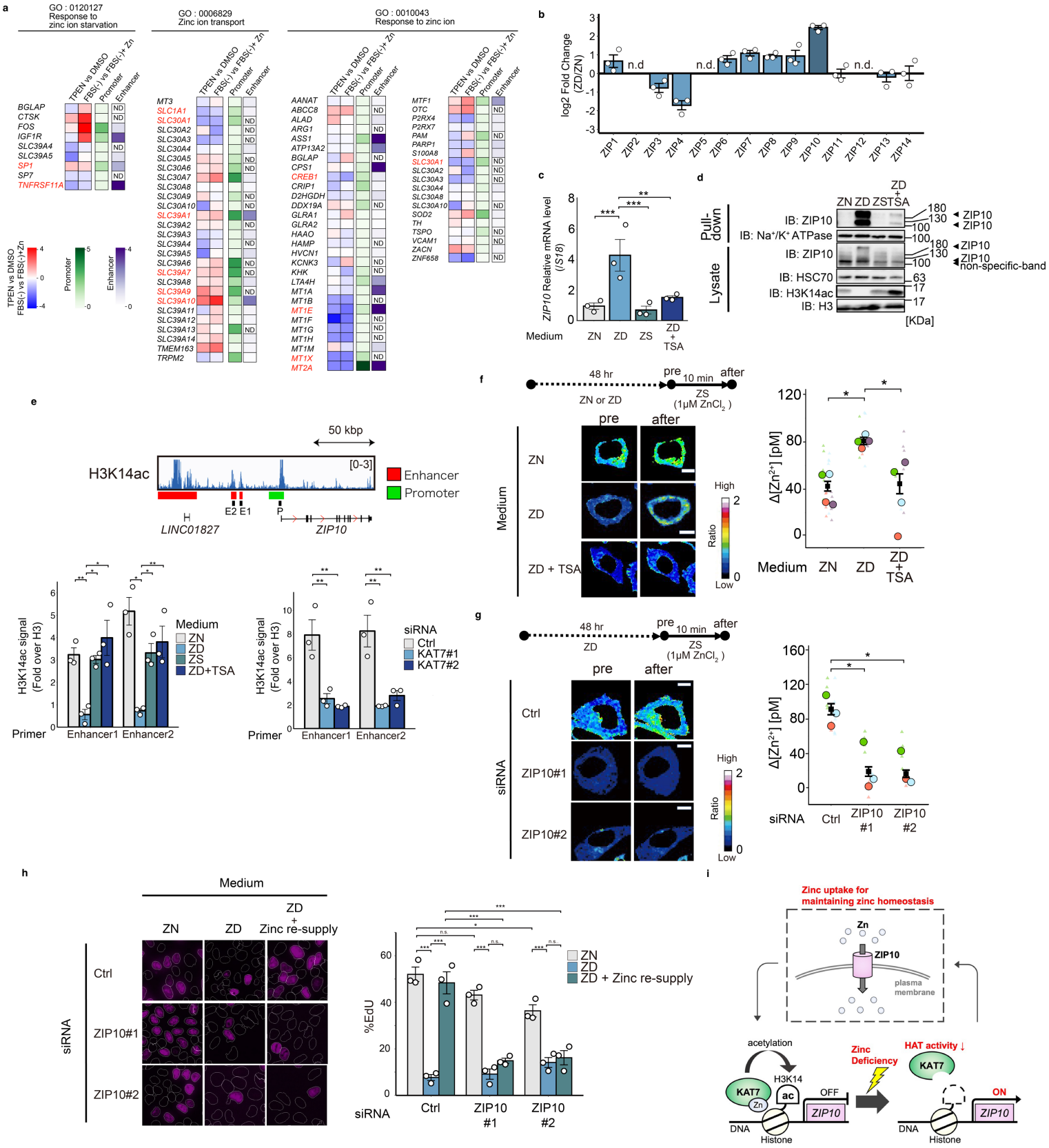
a
GO : 0120127
Response to
zinc ion starvation
GO : 0006829
Zinc ion transport
GO : 0010043
Response to zinc ion
TPEN vs DMSO
FBS(-) vs FBS(-)+ Zn
Promoter
Enhancer
BGLAP
CTSK
FOS
IGF1R
SLC39A4
SLC39A5
SP1
SP7
TNFRSF11A
MT3
SLC1A1
SLC30A1
SLC30A2
SLC30A3
SLC30A4
SLC30A5
SLC30A6
SLC30A7
SLC30A8
SLC30A9
SLC30A10
SLC39A1
SLC39A2
SLC39A3
SLC39A4
SLC39A5
SLC39A6
SLC39A7
SLC39A8
SLC39A9
SLC39A10
SLC39A11
SLC39A12
SLC39A13
SLC39A14
TMEM163
TRPM2
AANAT
ABCC8
ALAD
ARG1
ASS1
ATP13A2
BGLAP
CPS1
CREB1
CRIP1
D2HGDH
DDX19A
GLRA1
GLRA2
HAAO
HAMP
HVCN1
KCNK3
KHK
LTA4H
MT1A
MT1B
MT1E
MT1F
MT1G
MT1H
MT1M
MT1X
MT2A
MTF1
OTC
P2RX4
P2RX7
PAM
PARP1
S100A8
SLC30A1
SLC30A2
SLC30A3
SLC30A4
SLC30A8
SLC30A10
SOD2
TH
TSPO
VCAM1
ZACN
ZNF658
ND
b
log2 Fold Change
(ZD/ZN)
n.d
ZIP1
ZIP2
ZIP3
ZIP4
ZIP5
ZIP6
ZIP7
ZIP8
ZIP9
ZIP10
ZIP11
ZIP12
ZIP13
ZIP14
c
ZIP10 Relative mRNA level
(/S18)
Medium
ZN
ZD
ZS
ZD
+
TSA
d
Pull-down
Lysate
ZN ZD ZS TSA
ZD
+
IB: ZIP10
IB: Na+/K+ ATPase
IB: ZIP10
IB: HSC70
IB: H3K14ac
IB: H3
ZIP10
ZIP10
ZIP10
ZIP10
non-specific-band
[KDa]
e
50 kbp
H3K14ac
[0-3]
Enhancer
Promoter
H
E2 E1
P
LINC01827
ZIP10
H3K14ac signal
(Fold over H3)
Medium
ZN
ZD
ZS
ZD+TSA
Primer
Enhancer1
Enhancer2
siRNA
Ctrl
KAT7#1
KAT7#2
f
48 hr
pre
10 min
after
ZN or ZD
ZS
(1μM ZnCl2)
pre
after
Medium
ZN
ZD
ZD + TSA
High
Ratio
Low
Δ[Zn2+] [pM]
Medium
ZN
ZD
ZD
+
TSA
g
48 hr
pre
10 min
after
ZD
ZS
(1μM ZnCl2)
pre
after
siRNA
Ctrl
ZIP10#1
ZIP10#2
High
Ratio
Low
Δ[Zn2+] [pM]
siRNA
Ctrl
ZIP10
#1
ZIP10
#2
h
Medium
ZN
ZD
ZD
+
Zinc re-supply
siRNA
Ctrl
ZIP10#1
ZIP10#2
%EdU
ZN
ZD
ZD + Zinc re-supply
siRNA
Ctrl
ZIP10
#1
ZIP10
#2
i
Zinc uptake for
maintaining zinc homeostasis
Zn
ZIP10
plasma
membrane
acetylation
H3K14
ac
KAT7
Zn
OFF
ZIP10
DNA
Histone
Zinc
Deficiency
HAT activity ↓
KAT7
ON
ZIP10
DNA
Histone

Figure legends

Fig.1 Global decrease in histone H3K14ac during zinc deficiency

a Immunoblot analysis of HEK293A cells treated with TPEN for the indicated times. Representative of three independent experiments.

b Immunoblot analysis of HEK293A cells cultured in the indicated medium.

c Immunoblot analysis of HEK293A cells cultured in the indicated medium supplemented with each metal at 20 μM for 48 hours.

d Immunoblot analysis of HEK293A cells cultured in zinc-deficient medium supplemented with the indicated concentration of zinc for 48 hours. The graph shows the mean ± SEM of the H3K14ac level normalized to H3. The value of the H3K14ac level cultured in zinc-normal medium was normalized to 1. x-axis, logarithmic scale. The results of statistical analysis comparing a reference group (ZD, no zinc supplementation) to other groups are shown. $^{**}P < 0.01$, $^{***}P < 0.001$ by one-way ANOVA with Student's t test followed by Bonferroni post hoc correction. n.s. not significant.

e Immunoblot analysis of HEK293A cells cultured in zinc-deficient medium for 36 hours and additional cultures for the indicated times supplemented with 20 μM zinc. The graph shows the mean ± SEM of the H3K14ac level normalized to H3. The value of the H3K14ac level cultured in zinc-normal medium was normalized to 1. Data at time points 0.25 h and 0.5 h were omitted from the graph to avoid complexity. The omitted data from the graph were included in the following statistical analysis. The results of statistical analysis comparing a reference group (ZD, no zinc re-supply) to other groups are shown. $^{*}P < 0.05$, $^{***}P < 0.001$ by one-way ANOVA with Student's t test followed by Bonferroni post hoc correction. n.s. not significant.

Fig.2 HDACs deacetylate H3K14ac during zinc deficiency

a. Immunoblot analysis of HEK293A cells treated with 10 μM TPEN for two hours after pretreatment with NAM for one hour. Representative of three independent experiments.

b. Immunoblot analysis of HEK293A cells treated with 10 μM TPEN for two hours after pretreatment with TSA for one hour. Representative of three independent

experiments.

c. Immunoblot analysis of HEK293A cells. Cells were treated with the indicated siRNA and cultured for 48 hours. The cells were treated with 10 μM TPEN for the indicated times and subjected to immunoblot analysis. Representative of three independent experiments.

d. *In vitro* HDAC assay. Cell lysates treated with 10 μM TPEN for the indicated times were prepared. The lysates were incubated with purified histones with or without 2 nM TSA for the indicated times. The graph shows the mean ± SEM of the H3K14ac level normalized to H3. The value of the H3K14ac level incubated without cell lysate was normalized to 1. The results of statistical analysis comparing a reference group (no lysate) to other groups are shown on the bars. The results of statistical analysis comparing data from the same incubation times with lysate are also shown. ***$P < 0.001$ by one-way ANOVA with Student's t test followed by Bonferroni post hoc correction. n.s. not significant.

Fig.3 Zinc coordination in the KAT7 MYST domain regulates HAT activity towards H3K14

a. Immunoblot analysis of HEK293A cells treated with the indicated siRNAs for 48 hours. Representative of three independent experiments.

b. *In vitro* HAT assay. FLAG-KAT7 immunoprecipitated from HEK293A cells transfected with the indicated plasmids and treated with or without 10 μM TPEN for two hours was subjected to an *in vitro* HAT assay.

c. Upper panels, *in vitro* HAT assay. FLAG-KAT7 WT immunoprecipitated from HEK293A cells cultured in the indicated medium for 48 hours was subjected to *in vitro* HAT assay. Lower panels, immunoblot analysis of HEK293A cells transfected with FLAG-KAT7 WT and incubated with the indicated medium. ZN, zinc-normal medium; ZD, zinc-deficient medium; ZS, zinc deficient medium supplemented with 20 μM $ZnCl_2$. Representative of three independent experiments.

d. Left, schematic representation of the KAT7 domain structure and amino acid sequences in zinc finger domains. Right, 3D structures of the KAT7 MYST domain (Protein Data Bank, 6MAJ). Blue, zinc finger domain. The amino acids coordinating zinc are highlighted.

e. *In vitro* HAT assay. FLAG-KAT7 WT or mutants immunoprecipitated from

HEK293A cells were subjected to an *in vitro* HAT assay. Representative of three independent experiments.

f. *In vitro* HAT assay. recKAT7^{HAT} with or without mutation was subjected to HAT assay. Representative of three independent experiments.

g. ZnAF-2 assay. The zinc content in recKAT7^{HAT} was measured. The graph shows the mean ± SEM (n=3). ***$P < 0.001$ by one-way ANOVA with Student's t test followed by Bonferroni post hoc correction. n.s. not significant.

h. *In vitro* HAT assay. FLAG-KAT7 WT or C371A immunoprecipitated from HEK293A cells treated with or without 10 μM TPEN for two hours was incubated with the indicated concentration of $ZnCl_2$ for 30 min. The samples were subjected to an *in vitro* HAT assay. The results of statistical analysis comparing a reference group (no additional zinc) to other groups are shown on the plots. The results of statistical analysis comparing to data collected following 10 pM zinc supplementation are also shown. *$P < 0.05$, ***$P < 0.001$ by one-way ANOVA with Student's t test followed by Bonferroni post hoc correction. n.s., not significant.

Fig.4 Loss of H3K14ac on the enhancer induces *ZIP10* expression to maintain cellular zinc homeostasis

a. Heatmaps showing gene expression changes during zinc deficiency and the H3K14ac signal on promoter or enhancer regions. Genes in red character are possible candidates regulated by the decrease in H3K14ac during zinc deficiency, as defined by the following criteria: a fold change in expression of > 1.5 (upregulation or downregulation, data from GSE49657) and the promoter H3K14ac signal > 1.0 or the enhancer H3K14ac signal > 1.0. ND, not determined (no enhancer information on FANTOM5).

b. Quantitative PCR analysis of HeLa cells cultured in the indicated medium for 48 hours. The graph shows the mean ± SEM (n=3). n.d., not detected.

c. Quantitative PCR analysis of HeLa cells cultured in the indicated medium supplemented with 10 μM $ZnCl_2$ or 0.5 μM TSA for 36 hours. TSA was added every 12 hours. The graph represents mean ± SEM (n=3). **$P < 0.01$, ***$P < 0.001$ by one-way ANOVA followed by Dunnett's multiple comparison test.

d. Membrane protein biotinylation assay and immunoblot analysis of HeLa cells

cultured in the indicated medium supplemented with 10 μM $ZnCl_2$ or 0.5 μM TSA for 48 hours. TSA was added every 12 hours. Representative of three independent experiments. Immunoblot for Na^+/K^+ ATPase was performed to show the amount of membrane proteins.

e. Upper, H3K14ac ChIP-seq data. Enhancer regions deposited on EnhancerAtlas2.0 around *ZIP10*, the promoter region of *ZIP10*, and the regions used to design primers for ChIP–qPCR are shown. E1, Enhancer region 1; E2, Enhancer region 2; P, Promoter region. Lower, ChIP–qPCR analysis of HeLa cells cultured in the indicated medium supplemented with 10 μM $ZnCl_2$ or 0.5 μM TSA for 36 hours. TSA was added every 12 hours. The graph shows the mean ± SEM (n=3) of H3K14ac ChIP-qPCR signal normalized to H3 ChIP-qPCR signal. $*P < 0.05$, $**P < 0.01$ by one-way ANOVA with Student's t test followed by Bonferroni post hoc correction.

f. Left, pseudocolour fluorescence ratio images of ZnDA-3H/HTL-TMR. HeLa cells were cultured in the indicated medium for 12 hours. The cells were stimulated with 0.5 μM TSA for 36 hours. TSA was added every 12 hours. The difference in zinc concentration between before and 10 minutes after 1 μM zinc addition is shown. Scale bars, 10 μm. Representative of four independent experiments. Right, labile zinc influx in the cytoplasm measured by ZnDA-3H. A triangle indicates each datapoint, a circle indicates the mean of each experiment, and a rectangle indicates the mean of all experiments. The bar represents the mean ± SEM. Data for ZN (n=22), ZD (n=17), and ZD+TSA (n=12) were obtained from 4 independent experiments. $*P < 0.05$ by one-way ANOVA followed by Dunnett's multiple comparison test.

g. Left, pseudocolour fluorescence ratio images of ZnDA-3H/HTL-TMR. HeLa cells were treated with the indicated siRNA for 24 hours. The cells were cultured in zinc-deficient medium for an additional 48 hours. The difference in zinc concentration between before and 10 minutes after 1 μM zinc addition is shown. Scale bars, 10 μm. Representative of three independent experiments. Right, labile zinc influx in the cytoplasm measured by ZnDA-3H. A triangle indicates each datapoint, a circle indicates the mean of each experiment, and a rectangle indicates the mean of all experiments. The bar represents the mean ± SEM. Data for Ctrl (n=13), ZIP10#1 (n=18), and ZIP10#2 (n=17) were obtained from 3 independent

experiments. *$P < 0.05$ by one-way ANOVA followed by Dunnett's multiple comparison test.

h. EdU assay. HeLa cells treated with the indicated siRNA were cultured in the indicated medium for 48 hours. After incubation with or without 10 μM $ZnCl_2$ for 9 hours, an EdU assay was conducted. The graph represents mean ± SEM (n=3). *$P < 0.05$, ***$P < 0.001$ by one-way ANOVA with Student's t test followed by Bonferroni post hoc test. n.s., not significant.

i. A schematic of the model reported in this study.
ZN, zinc-normal medium; ZD, zinc-deficient medium; ZS, zinc deficient medium supplemented with 10 μM $ZnCl_2$.

Extended Data Fig. 1

a

GEO accession	Cell	Method	Number of upregulated genes	Number of upregulated genes with ERSE	% of upregulated genes with ERSE
GSE49657	HeLa	TPEN	1196	14	1.17
GSE99204	keratinocyte	TPEN	2230	10	0.45
GSE108923	HEK293 freestyle	Culture in zinc-depleted medium	1144	4	0.35
GSE135873	Caco-2	TPEN	285	2	0.70

b

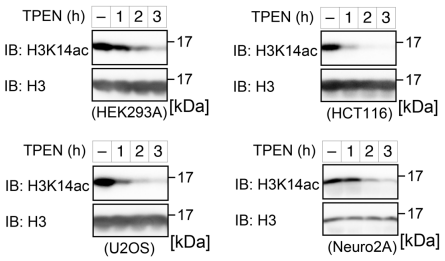

c

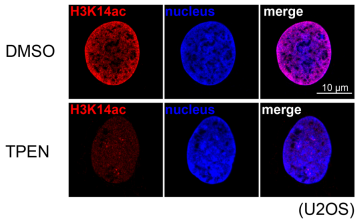

Extended Data Fig. 2

a

inhibitor	Target
TMP195	HDAC4 HDAC5 HDAC7 HDAC9
Tubastatin	HDAC6
UF010	HDAC1 HDAC2 HDAC3 HDAC6 HDAC8 HDAC10
MS275	HDAC1 HDAC2 HDAC3 HDAC8
SAHA	All HDACs
TSA	All HDACs

b

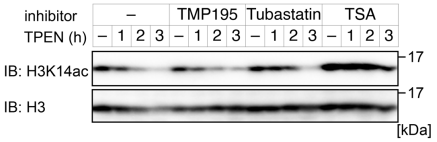

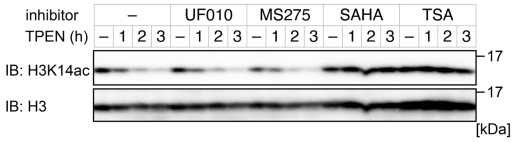

Extended Data Fig. 3

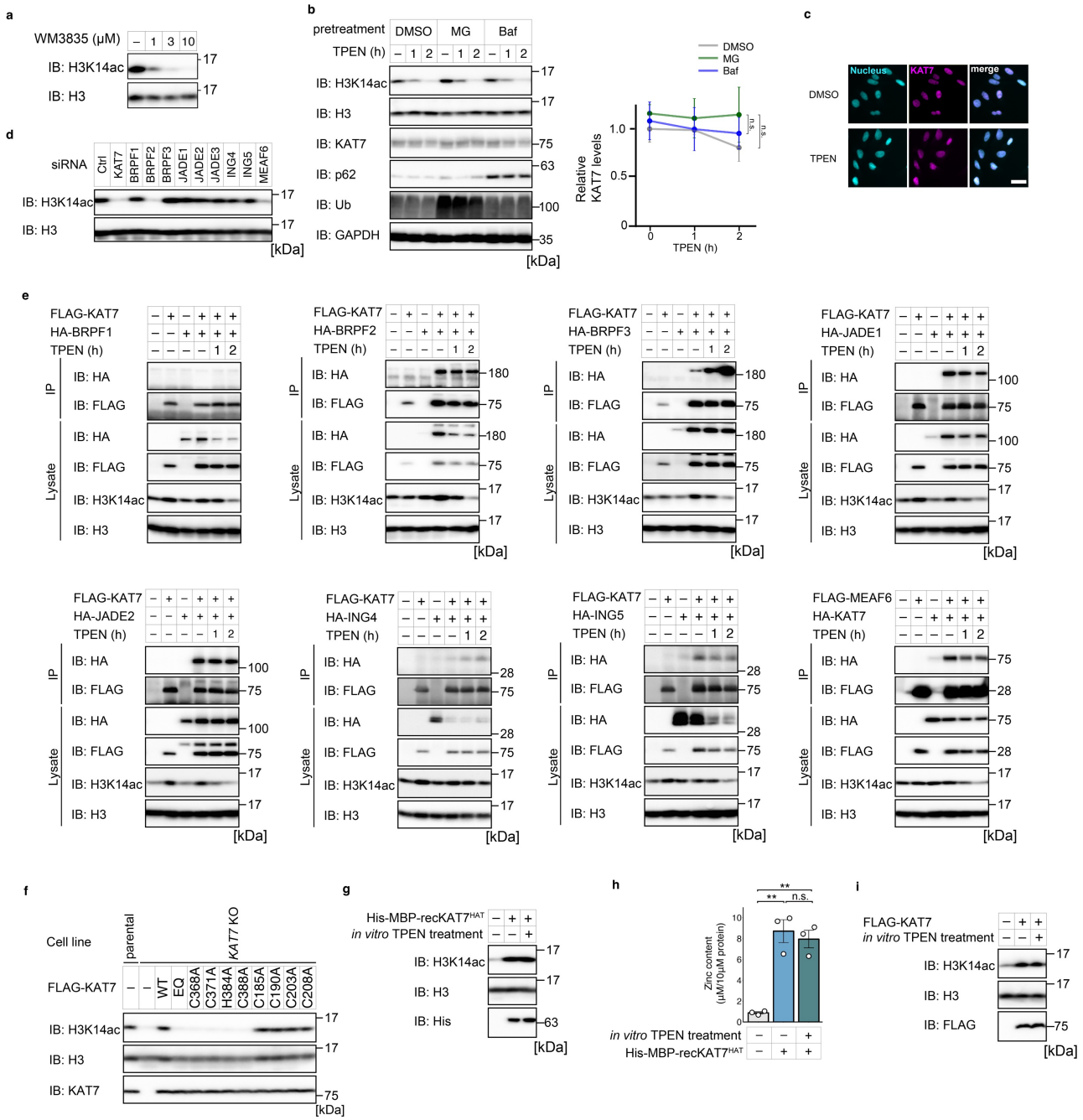

Extended Data Fig. 4

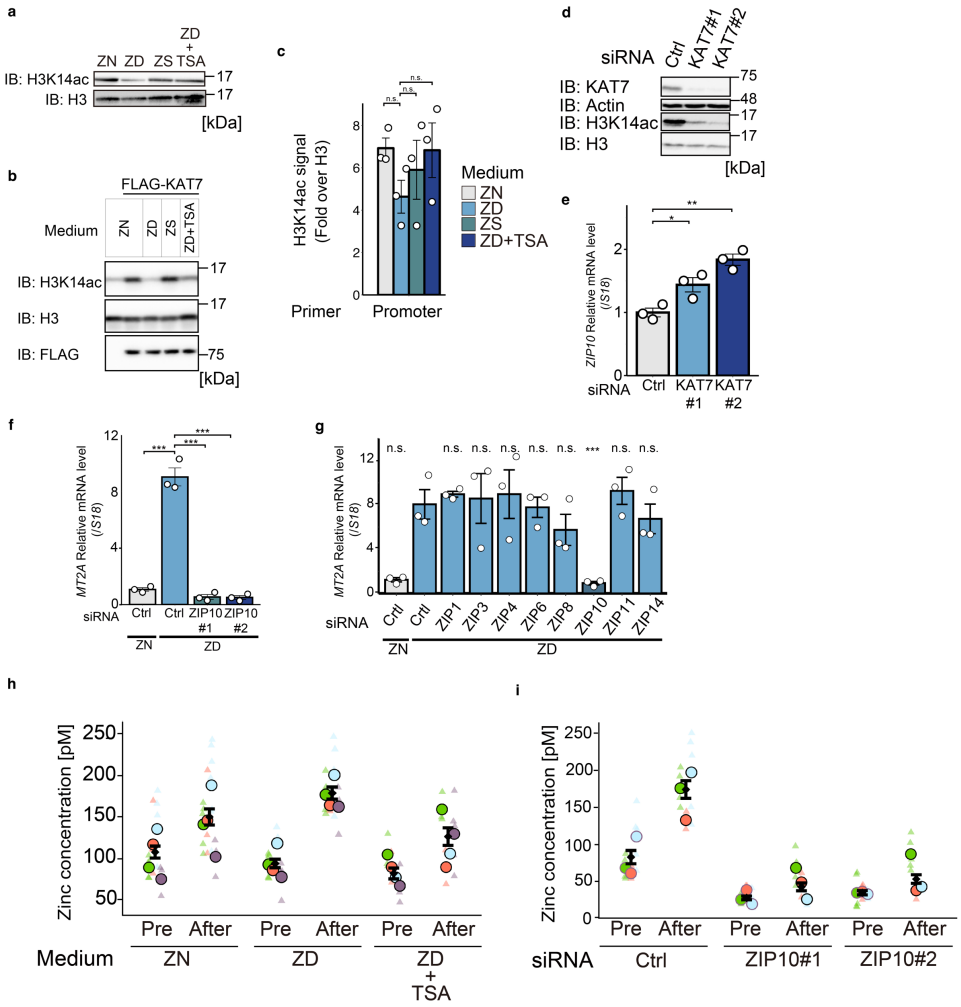

Extended Data Fig.1 Global decrease in histone H3K14ac during zinc deficiency

a. Analysis of the presence of the ATF6-interacting motif (ERSE) on promoters of the genes that were upregulated under zinc-deficient conditions.
b. Immunoblot analysis of cells treated with 10 μM TPEN for the indicated times. Representative of three independent experiments.
c. Immunofluorescence analysis of U2OS cells treated with 10 μM TPEN for two hours. Representative of three independent experiments. Thirty-two (DMSO) or 49 (TPEN) cells pooled from n = 3 experiments were analysed. Scale bar, 10 μm

Extended Data Fig.2 HDACs deacetylate H3K14ac during zinc deficiency

a. Classic HDAC members and their inhibitors.
b. Immunoblot analysis of HEK293A cells treated with 10 μM TPEN for the indicated times after pretreatment with HDAC inhibitors for 30 min. Representative of three independent experiments.

Extended Data Fig.3 Zinc coordination in the KAT7 MYST domain regulates HAT activity towards H3K14

a. Immunoblot analysis of HEK293A cells treated with WM-3835 for the indicated concentration for 24 hours. Representative of three independent experiments.
b. Immunoblot analysis of HEK293A cells treated with 10 μM TPEN for the indicated times after pretreatment with 1 μM MG132 (MG) or 50 nM bafilomycin A1 (Baf) for one hour. Immunoblotting for Ub was performed to show the effect of MG132. Immunoblotting for p62 was performed to show the effect of bafilomycin. Representative of three independent experiments. The graph show the mean ± SEM of the KAT7 level normalized to GAPDH. The value of the KAT7 level after pretreatment with DMSO was normalized to 1. The results of statistical analysis comparing a reference group (pretreatment with DMSO, two-hour TPEN treatment) to other groups at the same time point are shown. One-way ANOVA with Student's t test followed by Bonferroni post hoc correction. n.s., not significant.
c. Immunofluorescence analysis of U2OS cells treated with 10 μM TPEN for two hours. Representative of three independent experiments. A total of 142 (DMSO) or 145 (TPEN) cells pooled from n = 3 experiments were analysed. Scale bar, 10 μm.

d. Immunoblot analysis of HEK293A cells treated with the indicated siRNA for 48 hours. Representative of three independent experiments.
e. Coimmunoprecipitation analysis showing the interaction between KAT7 and the indicated protein. HEK293A cells were transfected with the indicated plasmids. After 10 μM TPEN treatment for the indicated times, samples were subjected to coimmunoprecipitation analysis. Data showing the interaction between KAT7 and JADE3 are not included due to the low expression of JADE3. Representative of three independent experiments.
f. Immunoblot analysis of HEK293A cells and HEK293A *KAT7* KO cells transfected with the indicated plasmids. Representative of three independent experiments.
g. *In vitro* HAT assay. recKAT7^{HAT} was incubated with or without 10 μM TPEN for two hours *in vitro*. Then the samples were subjected to the HAT assay. Representative of three independent experiments.
h. ZnAF-2 assay. The zinc content in recKAT7^{HAT} treated with 10 μM TPEN for two hours *in vitro* was measured. The graph represents mean ± SEM (n=3). $^{**}P < 0.01$ by one-way ANOVA with Student's t test followed by Bonferroni post hoc test. n.s. not significant.
i. *In vitro* HAT assay. FLAG-KAT7 WT immunoprecipitated from HEK293A cells was incubated with or without 10 μM TPEN for two hours *in vitro*. Then the samples were subjected to the HAT assay. Representative of three independent experiments.

Extended Data Fig.4 Loss of H3K14ac on the enhancer induces *ZIP10* expression to maintain cellular zinc homeostasis

a. Immunoblot analysis of HeLa cells cultured or treated with the indicated conditions. TSA was added every 12 hours. Representative of three independent experiments.
b. *In vitro* HAT assay. FLAG-KAT7 WT immunoprecipitated from HeLa cells cultured or treated under the indicated conditions was subjected to an *in vitro* HAT assay. TSA was added every 12 hours. Representative of three independent experiments.
c. ChIP–qPCR analysis of HeLa cells cultured in the indicated medium for 48 hours. TSA was added every 12 hours. The graph represents mean ± SEM (n=3). n.s. not

significant.

d. Immunoblot analysis of HeLa cells treated with the indicated siRNAs for 48 hours. Representative of three independent experiments.

e. Quantitative PCR analysis of HeLa cells treated with the indicated siRNAs for 48 hours. The graph represents mean ± SEM (n=3). *$P < 0.05$ and **$P < 0.01$ by one-way ANOVA with Dunnett's multiple comparison test.

f. Quantitative PCR analysis. HeLa cells treated with the indicated siRNAs for 24 hours were cultured in the indicated medium for 48 hours. After additional culture with medium supplemented with 1 μM $ZnCl_2$ for 60 min, the samples were subjected to quantitative PCR analysis. The graph represents mean ± SEM (n=3). ZN, zinc-normal medium; ZD, zinc-deficient medium. ***$P < 0.001$ by one-way ANOVA followed by Dunnett's multiple comparison test.

g. Quantitative PCR analysis. HeLa cells were treated with the indicated siRNAs for 48 hours. The cells were cultured in zinc-deficient medium for 48 hours, and after additional culture with medium supplemented with 1 μM $ZnCl_2$ for 60 min, the cells were subjected to quantitative PCR analysis. The graph show the mean ± SEM (n=3). ***$P < 0.001$ by one-way ANOVA followed by Dunnett's multiple comparison test. The results of statistical analysis comparing a reference group (ZD, Ctrl) to other groups are shown. n.s., not significant.

h. Labile zinc concentration in the cytoplasm measured by ZnDA-3H. A triangle indicates each datapoint, a circle indicates the mean of each experiment, and a rectangle indicates the mean of all experiments. The bar represents the mean ± SEM. Data for NZ (n=22), ZD (n=17), and ZD+TSA (n=12) were obtained from 4 independent experiments. pre, before zinc supplementation; after, 10 min after zinc supplementation.

i. Labile zinc concentration in the cytoplasm measured by ZnDA-3H. A triangle dot indicates each datapoint, a circle indicates the mean of each experiment, and a rectangle dot indicates the mean of all experiments. The bar represents the mean ± SEM. Data for Ctrl (n=13) , ZIP10#1 (n=18), and ZIP10#2 (n=17) were obtained from 3 independent experiments. pre, before zinc supplementation; after, 10 min after zinc supplementation.

ZN, zinc-normal medium; ZD, zinc-deficient medium; ZS, zinc deficient medium supplemented with 10 μM $ZnCl_2$.

Table 1. A list of primers and siRNAs used in this study

RT-qPCR

Primer Name	**Sequence (5'-3')**
S18_for	TTTGCGAGTACTCAACACCAA
S18_rev	GCATATCTTCGGCCCACA
ZIP1_for	CAGGGCCTCATCTATGGCA
ZIP1_rev	TGAGCCTAGTAAGCTGTTTCGC
ZIP2_for	CTGCTGGAGGATCGACAGTG
ZIP2_rev	CACAAGCCCCTTATGAGCCA
ZIP3_for	TGCTCCCCCGTGAAGATCATC
ZIP3_rev	TCCAAAGGTGTTGCAGAGAGA
ZIP4_for	TGGTCTCTACGTGGCACTC
ZIP4_rev	GGGTCCCGTACTTTCAACATC
ZIP5_for	GGTCCCCAGTGAGTCATCTG
ZIP5_rev	GCCAGGTAATGGTTCTGCTCC
ZIP6_for	ATGCAAGTCACCACCATAGTCA
ZIP6_rev	ACGTGGAATCAAAATAGGCACT
ZIP7_for	GGACACGCTCACAGTCATACA
ZIP7_rev	CTCCTCGCCTCTTCTGAACC
ZIP8_for	ATGCTACCCAAATAACCAGCTC
ZIP8_rev	ACAGGAATCCATATCCCCAAACT
ZIP9_for	CATGCTGGCTTAGAGCGGAAT
ZIP9_rev	TGGTGCTGCCAATGCAAAGA
ZIP10_for	TTTCACTCACATAACCACCAGC
ZIP10_rev	GTGATGACGTAGGCGGTGATT
ZIP11_for	CAGCTCTCGTGTTCGTATTCTC
ZIP11_rev	TCAGCCAAGTAGACAAAAGCC
ZIP12_for	TTCTTCTACTCAGCCGTGTTTTT
ZIP12_rev	GTCACCAGCAGAGAGAACCT
ZIP13_for	TCAGCGGCTACCTCAACCT
ZIP13_rev	AGGAGCCCGATCTTCTTGCT
ZIP14_for	GAGGCTCACGCTTCATCCC

ZIP14_rev	CCCTCGCCATACCGATGTATTA
MT2A_for	AGCCAAGCGGCCTAAACTC
MT2A_rev	TCACCACCATTGGTTAGTCCC

ChIP-qPCR

Primer Name	**Sequence (5'-3')**
Enhancer1_for	TGCAAAACTTCCTGAGGTGA
Enhancer1_rev	ATGGCAGTATTTGCGGTAGG
Enhancer2_for	GGAAAATAGAGGGGGTCTGG
Enhancer2_rev	CAGTGTGGACCAGCAACATC
Promoter_for	GCAAGAATGAGCACGGTGTA
Promoter_rev	AGCACACTTACTGCGGGTCT

Cloning

Primer Name	**Sequence (5'-3')**
KAT7_for	GATGACAAGGGCGAATTCATGCCGCGAAGGAAGAGG
KAT7_rev	ATAGGGCCCTCTAGATTAAGTGCCCTTGGGAGGGG
BRPF1_for	AGCCTCGGCGAATTCATGGGGGTGGACTTTGAT
BRPF1_rev	AGATGCATGCTCGAGTTAATCACTATCGCTGGTC
BRPF2_for	AGCCTCGGCGAATTCATGAGGAGGAAAGGACG
BRPF2_rev	AGATGCATGCTCGAGTTAGTCAATGTCACTGAGG
BRPF3_for	AGCCTCGGCGAATTCATGAGGAAGCCTCGTCGG
BRPF3_rev	AGATGCATGCTCGAGTTACAGGTAGCTGGAAGTG
JADE1_for	AGCCTCGGCGAATTCATGAAACGAGGTCGCCTT
JADE1_rev	AGATGCATGCTCGAGTTAAGAAGCCAAGATGCTT
JADE2_for	AGCCTCGGCGAATTCATGGAAGAGAAGAGGCGA
JADE2_rev	AGATGCATGCTCGAGTTAGGAGGCCAGTACGCCC
JADE3_for	AGCCTCGGCGAATTCATGAAACGCCATAGGCCT
JADE3_rev	AGATGCATGCTCGAGTTACCTTTGCATTGAACTG
ING4_for	AGCCTCGGCGAATTCATGGCTGCGGGGATGTAT
ING4_rev	AGATGCATGCTCGAGTTATTTCTTCTTCCGTTCT
ING5_for	AGCCTCGGCGAATTCATGGCGACCGCCATGTAC

ING5_rev	AGATGCATGCTCGAGTTACTTCTTCTTCCTCTTT
MEAF6_for	GACAAGGGCGAATTCATGGCGATGCACAACAAG
MEAF6_rev	AGATGCATGCTCGAGTTAATAGTCAGCTCGTGGT

Mutagenesis

Primer Name	**Sequence (5'-3')**
C185A_for	TATGAAGGCTCCTACACCAGGCTGTAA
C185A_rev	TGTAGGAGCCTTCATATTGAAGTTGTA
C190A_for	CCAGGCGCTAACTCTCTAGGACACCT
C190A_rev	AGAGTTAGCGCCTGGTGTAGGACACTT
H203A_for	TGAGAGAGCTTTCTCCATCTCAGGATG
H203A_rev	GGAGAAAGCTCTCTCATGTTTTCCT
C209A_for	CTCAGGAGCCCCACTGTATCATAACCT
C209A_rev	CAGTGGGGCTCCTGAGATGGAGAAATG
C368A_for	CTATATGGCTGAATTCTGTTTAAAATA
C368A_rev	AGAATTCAGCCATATAGAGACGTCCCA
C371A_for	TGAATTCGCTTTAAAATATATGAAGAG
C371A_rev	ATTTTAAAGCGAATTCACACATATAGA
H384A_for	CCGCCGGGCCATGGCCAAATGTGTGTG
H384A_rev	TGGCCATGGCCCGGCGGAGTATCGTTT
C388A_for	GGCCAAAGCTGTGTGGAAACACCCACC
C388A_rev	TCCACACAGCTTTGGCCATGTGCCGGC
E508Q_for	CTCCCCACAACGTCCACTCTCAGATCT
E508Q_rev	GTGGACGTTGTGGGGAGCCAACTTTTT

siRNA

Catalog Number	**Gene Symbol**	**Sequence (5'-3')**
J-017668-05	KAT7	GAACCGAAGAUUCCGAUUU
J-017668-07	KAT7	UAGGACACCUUACAGGAAA
J-007565-17	ZIP10	CCACAAACCUGAUCGUGUA
J-007565-18	ZIP10	UGCAUUAGCUGUAGGAACA